

1 Manuscript No.: **acp-2017-165**

2 Journal: **ACP**

3 The revised manuscript entitled “**Measurement of scattering and absorption**  
4 **properties of dust aerosol in a Gobi farmland region of northwest China—a**  
5 **potential anthropogenic influence**” by Jianrong Bi, et al.

6

7 **Response to Referee#1:**

8 We are grateful to the Editor’s and Referee#1’s insightful and constructive comments  
9 for this manuscript! We have carefully checked and revised the whole manuscript  
10 according to Referee#1’s comments, which are helpful and valuable for greatly  
11 improving our manuscript. Please find a point-by-point reply to the issues as follows  
12 (highlighted in the blue font). And we have also uploaded the file of “Response  
13 to-Referee#1(acp-2017-165).pdf”.

14

15 **General comments:**

16 Dust aerosol in remote Taklimakan Desert and Gobi deserts of northwest China is  
17 thought to be hardly affected by human activities, due to sparse population. The  
18 authors conducted a comprehensive field measurement in a Gobi farmland region of  
19 northwest China, and demonstrated a potential anthropogenic influence on dust  
20 physicochemical properties using multiple ground-based active and passive sensors.  
21 The agricultural operations and biomass burning from crop residue prior to growing  
22 season were well documented to produce significant impacts on elevated dust  
23 loadings and absorption characteristics in Dunhuang farmland during spring of 2012.  
24 The findings of this study are very interesting and would help to improve our  
25 understanding of the interaction among dust aerosol, atmospheric chemistry, and  
26 climate change in desert source region. And I suggest that the authors should carry out  
27 long-term and continuous measurements of mineral dust at remote Gobi deserts in  
28 northwest China, to quantify the potential anthropogenic contributions on regional  
29 climatic and environmental changes. I think the English writing is fine, and I  
30 recommend this manuscript is appropriate for publishing after minor revision.

31 **Response:** Thank you very much for the Referee’s good suggestions and the  
32 acceptance of this work. Indeed, this study only covers several months in spring  
33 during intensive period and it is indispensable to acquire long-term measurements of  
34 mineral dust for fully understanding the potential anthropogenic contributions on  
35 regional environmental and climatic changes. Hence, we have set up two permanent  
36 field observatories (SACOL and Dunhuang) in northwest China to continuously  
37 measure mineral dust since 2013, and will obtain more valuable findings, which will  
38 help quantify the anthropogenic contributions of dust aerosol in remote desert source  
39 region.

40

41 **Minor comments:**

42 1. **Abstract**, Page 1, line 27: “In the afternoon (13:00–18:00 LT)”

43 ⇒ Change to “In the afternoon (13:00–18:00 LT, local time)”. When an abbreviation  
44 firstly appears in the manuscript, please give the full name.

45 **Response:** We have changed “In the afternoon (13:00–18:00 LT)” to “In the afternoon  
46 (13:00–18:00 LT, local time)” in Line 27 and modified the corresponding places in the  
47 entire context.

48

49 2. Page 3, line 78: “(i.e., hematite and goethite)”

50 ⇒ Change to “(i.e. hematite and goethite)”

51 **Response:** We have changed to “(i.e. hematite and goethite)” in Line 78.

52

53 3. Page 4, line 90: “(i.e., Mongolia Gobi desert)”

54 ⇒ Change to “(i.e. Inner Mongolian Gobi desert)”

55 **Response:** We have changed to “(i.e. Inner Mongolian Gobi desert)” in Line 90.

56

57 4. Page 4, line 111: “close to the east edge of Kumtag Desert”

58 ⇒ Change to “close to the eastern edge of Kumtag Desert”

59 **Response:** We have changed to “close to the eastern edge of Kumtag Desert” in Line  
60 111.

带格式的: 字体颜色: 蓝色

带格式的: 字体颜色: 蓝色

61

62 5. Page 5, line 130: “to the southeast”

63 ⇒ Change to “to the southwest”

64 **Response:** We have changed to “to the southwest” in Line 130.

65

66 6. Page 6, line 154: “High AI values (>0.7) distributions”

67 ⇒ Change to “The distributions of high AI values (>0.7)”

68 **Response:** We have changed “High AI values (>0.7) distributions” to “The  
69 distributions of high AI values (>0.7)” in Line 154.

70

71 7. Page 9, line 265: “(i.e., Mongolia cyclones)”

72 ⇒ Change to “(i.e. Mongolian cyclone)”

73 **Response:** We have changed “(i.e., Mongolia cyclones)” to “(i.e. Mongolian  
74 cyclone)” in Line 265.

75

76 8. Page 12, line 331: “2 to 4 km”

77 ⇒ Change to “4 km”

78 **Response:** We have changed “2 to 4 km” to “4 km” in Line 331.

79

80 9. Page 12, line 332: “which was within the planetary boundary layer (PBL)”

81 ⇒ Change to “which was above the planetary boundary layer (PBL)”

82 **Response:** We have changed to “which was above the planetary boundary layer  
83 (PBL)” in Line 332.

84

85 10. Page 14, line 402: “Likewise”

86 ⇒ Change to “Similarly”

87 **Response:** We have changed “Likewise” to “Similarly” in Line 402.

88

89 11. Page 19, line 563: “atmospheric boundary layer structure”

90 ⇒ Change to “the structure of atmospheric boundary layer”

带格式的: 字体颜色: 蓝色

91 **Response:** We have changed “atmospheric boundary layer structure” to “the structure  
92 of atmospheric boundary layer” in Line 563.

93

94 12. Page 20, line 575: “lager”

95 ⇒ Change to “larger”

96 **Response:** We have changed “lager” to “larger” in Line 575.

97

98 13. Page 21, line 614: “The findings of this study directly demonstrated mineral dust”

99 ⇒ Change to “The findings of this study directly demonstrated that mineral dust”

100 **Response:** We have changed to “The findings of this study directly demonstrated that  
101 mineral dust” in Line 614.

102

带格式的: 字体: 小四, 非加粗,  
字体颜色: 蓝色

103 **Response to Referee#2:**

104 We appreciate the Editor and Referee#2’s valuable and constructive comments for this  
105 manuscript, which greatly assist in improving the quality of the original manuscript!  
106 We have carefully checked and revised the whole manuscript according to  
107 Referee#2’s comments. Please find a point-by-point reply to the issues as follows  
108 (highlighted in the blue font). And we have also uploaded the file of  
109 ‘acp-2017-165-supplement.pdf’.

110

111 **General comments:**

112 This manuscript presents the measurement of scattering and absorption properties of  
113 dust aerosol from a comprehensive field campaign in a Gobi farmland region of  
114 northwest China during spring 2012. Overall, the manuscript could make a good  
115 contribution to the scientific research by providing useful scientific knowledge on the  
116 interaction among dust aerosol, atmospheric chemistry, and climate change in desert  
117 source region. However, I believe that the manuscript needs the following minor  
118 revisions before it is accepted for publication by ACP.

119 **Response:** Thank you very much for the Referee’s insightful suggestions and  
120 constructive comments on this manuscript. We have carefully checked and revised the

121 whole manuscript according to Referee#2's comments. Please find a point-by-point  
122 reply to the issues as follows.

123

124 **Minor comments:**

125 1. Lines 22–24: Please present the more results and discussions on the statement in  
126 the text about the statement in the abstract that “The anthropogenic dust produced by  
127 agricultural cultivations (e.g., land planning, plowing, and disking) exerted a  
128 significant superimposed effect on high dust concentrations in Dunhuang farmland  
129 prior to the growing season (i.e., from 1 April to May).”

130 **Response:** We have presented visual photos of a variety of agricultural cultivations in  
131 Dunhuang farmland (nearby SACOL's Mobile Facility) prior to the growing season (i.e.  
132 from 1 April to 10 May, 2012), as shown in Figure S1. Diverse agricultural operations  
133 (e.g., land planning, plowing, disking and laying plastic mulch) were carried out in  
134 loose and bare Dunhuang farmland from 1 April to 10 May, 2012, which produced  
135 massive soil dust into the atmosphere, especially under strong surface winds (see  
136 Figure S1a-c). Therefore, the mass concentrations of particulate matter (PM<sub>10</sub>) in the  
137 source and adjacent downwind regions (including SACOL's Mobile Facility) were  
138 significantly elevated by these human activities. In contrast, the crops in Dunhuang  
139 farmland gradually become green since 10 May, 2012, indicating the coming of  
140 growth season (Figure S1f).

141 We also added more discussions about this in the context (Page 10, Lines 272–278).

142 Please check our revised manuscript in detailed.

143

144 2. Lines 25–27: It is a misleading conclusion that “Strong south valley wind and  
145 vertical mixing in daytime scavenged the pollution and weak northeast mountain wind  
146 and stable inversion layer at night favorably accumulated the air pollutants near the  
147 surface.” Please follow the diurnal changes of winds and PM<sub>10</sub> in Figs. 4 and 6.

148 **Response:** Thank you very much for your suggestions! The conclusion here  
149 corresponds to the diurnal changes of winds and PM<sub>10</sub> in Figs. 4 and 6, which can be  
150 interpreted by classical mountain-valley wind circulation. Please refer to more

151 detailed explanations in Pages 12–13, Lines 336–359.

152

153 3. It could be unnecessary to present the wind fields at 500 hPa and 850 hPa levels  
154 from the MERRA reanalysis products in Fig. 7, because the dust aerosols in a Gobi  
155 farmland region of northwest China are mostly the local emissions and a  
156 short-distance transport to the measurement site within the boundary layer.

157 **Response:** Thank you very much for your good comments! We mainly intend to  
158 elucidate two points using Fig. 7. Firstly, the selected three heavy dust events (i.e. 30  
159 April, 1 May, and 10 June) were triggered by different synoptic cyclones. East Asian  
160 region was governed by the powerful and stable westerlies at 500 hPa height on 30  
161 April and 1 May 2012, whereas strong Mongolian cyclones at 500 hPa upper  
162 atmosphere hovered about the southern Mongolia on 10 June 2012. Secondly, the  
163 ground-based measured strong northeast and east winds ( $> 10 \text{ ms}^{-1}$ ) under three dust  
164 events were completely consistent with the wind fields at 850 hPa levels from the  
165 MERRA reanalysis products, which indicated the studied dust events were regional  
166 scales instead of local scales.

167

168 4. Line 532: “mesoscale cyclones” should be “synoptic cyclones”.

169 **Response:** We have changed “mesoscale cyclones” to “synoptic cyclones” in Line  
170 532.

171

172 5. Lines 570–577: It is an interesting result that Figure 10d displays that “the DLW  
173 values under dusty cases were always greater than that in clear-sky cases, with the  
174 total average differences of  $+40\sim+60 \text{ Wm}^{-2}$ ”. However, the interpretation is  
175 unconvinced. From Fig. 10d, it could be seen that the warming dust layer could  
176 enhance that surface DLW with a large ( $+40\sim+60 \text{ Wm}^{-2}$ : not a few percentages!)  
177 contribution to the increased DLW. It is unreasonable that the potential greenhouse  
178 gases in the atmosphere could substantially affect the DLW differences between dusty  
179 and clear-sky cases (Fig. 10d). Also, please present the measured cloud cover or RH  
180 on April 9 to support the statement that “it is partly attributable to the higher RH

181 values on 9 June than that in other days.”

182 **Response:** Thank you very much for your insightful and valuable comments! Indeed,  
183 the warming dust layer could enhance that surface DLW with a large contribution to  
184 the increased DLW (+40~+60 Wm<sup>-2</sup>: not a few percentages!). Hence, we have  
185 changed “contribute a few percentages to the increased DLW” to “contribute a large  
186 percentages to the increased DLW” in Line 576.

187 “the potential greenhouse gases in the atmosphere could substantially affect the DLW  
188 variations.”: “the greenhouse gases” in the manuscript represent the presence of water  
189 vapor or clouds in the atmosphere, which causes confusion. Therefore, we have  
190 changed “This is because the potential greenhouse gases in the atmosphere could  
191 substantially affect the DLW variations.” to “This is because the potential water vapor  
192 in the atmosphere could substantially affect the DLW variations.” in Lines 573-575.  
193 Meanwhile, we have presented the diurnal variations of 10-second average relative  
194 humidity (RH, %) under completely clear-sky conditions (14 May, 29 May, and 9  
195 June) and dust events (30 April and 10 June) in Dunhuang farmland, as shown in  
196 Figure S2. We can clearly see that the RH on 9 June keeps the highest value in the  
197 whole day, which is greater than that in other cloudless or dusty days.

198

199 6. Please improve the quality of all the Figs., with clarifying the figure captions,  
200 such as horizontal wind vector in Figs. 4, near surface wind in Figs. 6 and 8, and the  
201 same color curves for all the Figs. 10a, 10b, 10c and 10d.

202 **Response:** Thank you very much for your valuable comments for improving the  
203 quality of this manuscript! We have improved the quality of all the Figs. in the context  
204 and corrected the same color curves for all the Figs. 10a, 10b, 10c, and 10d. Please  
205 refer to the revised manuscript in detail.

206

207

208

209 **Measurement of scattering and absorption properties of dust aerosol**  
210 **in a Gobi farmland region of northwest China—a potential**  
211 **anthropogenic influence**

212 Jianrong Bi, Jianping Huang, Jinsen Shi, Zhiyuan Hu, Tian Zhou, Guolong Zhang,  
213 Zhongwei Huang, Xin Wang, and Hongchun Jin

214

215 Key Laboratory for Semi-Arid Climate Change of the Ministry of Education, College of  
216 Atmospheric Sciences, Lanzhou University, Lanzhou 730000, China

217

218 *Correspondence to:* Jianping Huang (hjp@lzu.edu.cn)

219

220 **Abstract.** We conducted a comprehensive field campaign on exploring the optical  
221 characteristics of mineral dust in Dunhuang farmland nearby the Gobi deserts of  
222 northwest China during spring of 2012. The day-to-day and diurnal variations of dust  
223 aerosol showed prominent features throughout the experiment, primarily attributable  
224 to frequent dust events and local anthropogenic emissions. The overall average mass  
225 concentration of the particulate matter with an aerodynamic diameter less than 10  $\mu\text{m}$   
226 ( $\text{PM}_{10}$ ), light scattering coefficient ( $\sigma_{\text{sp},670}$ ), absorption coefficient ( $\sigma_{\text{ap},670}$ ), and  
227 single-scattering albedo ( $\text{SSA}_{670}$ ) were  $113 \pm 169 \mu\text{g m}^{-3}$ ,  $53.3 \pm 74.8 \text{ Mm}^{-1}$ ,  $3.2 \pm 2.4$   
228  $\text{Mm}^{-1}$ , and  $0.913 \pm 0.05$ , which were comparable to the background levels in southern  
229 United States, but smaller than that in the eastern and other northwestern China. The  
230 anthropogenic dust produced by agricultural cultivations (e.g., land planning, plowing,  
231 and disking) exerted a significant superimposed effect on high dust concentrations in  
232 Dunhuang farmland prior to the growing season (i.e., from 1 April to 10 May). Strong  
233 south valley wind and vertical mixing in daytime scavenged the pollution and weak  
234 northeast mountain wind and stable inversion layer at night favorably accumulated the  
235 air pollutants near the surface. In the afternoon (13:00–18:00 LT, local time), mean  
236  $\text{SSA}_{670}$  was  $0.945 \pm 0.04$  that was predominant by dust particles, whereas finer



237 particles and lower  $SSA_{670}$  values ( $\sim 0.90$ – $0.92$ ) were measured at night, suggesting  
238 the potential influence by the mixed dust-pollutants. During a typical biomass burning  
239 event on 4 April 2012,  $\sigma_{ap,670}$  ~~changed-increased~~ from  $\sim 2.0 \text{ Mm}^{-1}$  to  $4.75 \text{ Mm}^{-1}$  and  
240  $SSA_{670}$  changed from  $\sim 0.90$  to  $\sim 0.83$ , implying remarkable modification of aerosol  
241 absorptive properties induced by human activities. The findings of this study would  
242 help to advance an in-depth understanding of the interaction among dust aerosol,  
243 atmospheric chemistry, and climate change in desert source region.

## 244 1. Introduction

245 Asian mineral dust (also known as dust aerosol) in the atmosphere is deemed to  
246 exert a profound impact on air quality and climate change. It can perturb the energy  
247 budget of the Earth system directly through scattering and absorption of solar and  
248 terrestrial radiation (Huang et al., 2009, 2014; Ge et al., 2010; Li et al., 2016) and  
249 indirectly by altering cloud microphysical processes and related hydrological cycle  
250 (Rosenfeld et al., 2001; J. Huang et al., 2005, 2006, 2010; Yin and Chen, 2007; W.  
251 Wang et al., 2010; Creamean et al., 2013; Wu et al., 2016), as well as modifying snow  
252 and ice surface albedo (Aoki et al., 2006; Huang et al., 2011; Wang et al., 2013; Qian  
253 et al., 2014). In addition, alkaline mineral dust carries abundant organic matters and  
254 iron ions deposited on the surface of earth, and hence affects biomass productivity ~~of~~  
255 in the North Pacific Ocean and relevant atmosphere-ocean carbon exchange, which  
256 plays a pivotal role in the global biogeochemical cycle and carbon cycle (Cao et al.,  
257 2005; Jickells et al., 2005; Maher et al., 2010; Shao et al., 2011).

258 The Taklimakan Desert in northwestern China and Gobi Deserts in southern  
259 Mongolia and northern China are widely regarded as two major active centers of dust  
260 storms in East Asia (Sun et al., 2001; Zhao et al., 2006; Wang et al., 2008; Ge et al.,  
261 2016). These extensive arid and desert zones frequently generate a great deal of tiny  
262 soil particles every spring that are uplifted and entrained into the free atmosphere  
263 layer via cold frontal cyclones (Zhang et al., 1997; Aoki et al., 2005; Kai et al., 2008;  
264 J. Huang et al., 2009, 2010, 2014). Affected by mid-latitude prevailing westerlies,  
265 these dust particles can transport long distances on a subcontinental scale, even sweep

266 across the remote Pacific Ocean and occasionally arrive at the west coast of North  
267 America during the peak seasons of strong dust storms (Zhao et al., 2006; Uno et al.,  
268 2009, 2011). They then have a far-reaching influence on climatic and environmental  
269 changes both regionally and globally. Until now, there have been a large number of  
270 intensive field experiments (e.g., ACE–Asia, ADEC, PACDEX, EAST–AIRC) and  
271 ground-based aerosol monitoring networks (e.g., AERONET, SKYNET, CARSNET)  
272 for probing the Asian mineral dust (Holben et al., 1998; Huebert et al., 2003;  
273 Nakajima et al., 2003; Takamura et al., 2004; Eck et al., 2005; Mikami et al., 2006;  
274 Huang et al., 2008a; Che et al., 2009, 2015; Li et al., 2011), which is crucial to aid in  
275 thoroughly understanding the climatic effects of dust aerosols over East Asian domain.  
276 Nevertheless, due to poorly sampled over desert source areas of northwest China, the  
277 light scattering and absorption properties of mineral dusts in this region are far  
278 inadequate and urgently need to be further surveyed.

279 The Intergovernmental Panel on Climate Change (IPCC, 2013) reported that the  
280 symbol and magnitude of the radiative forcing of mineral dust is greatly reliant on the  
281 accurate and reliable knowledge of aerosol total loading, microphysical and chemical  
282 characteristics, as well as its spatiotemporal distribution. The current consensus is that  
283 nearly pure dust aerosol in the globe has relatively low light-absorption, with  
284 single-scattering albedo of  $\sim 0.96\text{--}0.99$  (Dubovik et al., 2002; Anderson et al., 2003;  
285 Uchiyama et al., 2005; Bi et al., 2014, 2016), which ~~principally~~ depends principally  
286 on the fraction and mixing ways of ferric iron oxides (i.e., hematite and goethite) in  
287 dust (Sokolik and Toon, 1999; Lafon et al., 2004, 2006). However, the coexistences of  
288 both mineral dust and other types of aerosols originated from diverse human activities  
289 (e.g., coal combustion, mobile source emissions, and biomass burning) are ubiquitous  
290 in the real atmosphere, which increases the complexity and variability to aerosol key  
291 parameters (Arimoto et al., 2004; Xu et al., 2004; Wang et al., 2015). When the lofted  
292 dust plumes in desert source areas are traveled eastward across the polluted regions,  
293 they commonly mix with anthropogenic pollutants and enhance heterogeneous  
294 chemical reactions with other reactive gas species, and then may remarkably alter  
295 their chemical and microphysical properties (Arimoto et al., 2006; Li and Shao et al.,

296 2009; Nie et al., 2014). It is well documented that the mineral dust might have already  
297 mixed with polluted aerosols in near dust source regions of northwest China (i.e.;  
298 Inner Mongolian Gobi desert), besides the mixing processes on the transport pathway  
299 (K. Huang et al., 2010). Xu et al. (2004) indicated that both dust aerosol and local  
300 pollution sources coexisted in Yulin nearby the Mu Us desert of northwest China  
301 during April 2001, which produced a significant influence on aerosol properties in the  
302 region. Likewise, Li et al. (2010) analyzed trace gases and aerosols observed at  
303 Zhangye (39.082°N, 100.276° E, 1460 m above MSL), a rural site within the Hexi  
304 Corridor in northwest China during spring 2008, and uncovered that the mixing  
305 between mineral dust and anthropogenic air pollutants can be omnipresent in this area,  
306 including at nighttime or during severe dust events. It implies that prior to moving out  
307 from the source region, dust particles were likely in connection with pollutants. For  
308 the sparsely populated and lesser anthropogenic affected desert source regions in  
309 northwest China (e.g., the Taklimakan Desert and its adjacent areas), the interaction  
310 between local pollutions and mineral dust is deserved to explore in depth. This is of  
311 prime importance to ascertain the relative contributions of two different aerosol  
312 sources in atmospheric chemistry and regional climate change.

313 To advance a better understanding of the drought processes and dust-relevant  
314 climatic impacts in northwest China (Huang et al., 2008b; Bi et al., 2011; G. Wang et  
315 al., 2010), the Semi-Arid Climate and Environment Observatory of Lanzhou  
316 University (henceforth referred to as SACOL, <http://climate.lzu.edu.cn/english/>)  
317 carried out a comprehensive field campaign in Dunhuang during spring of 2012.  
318 Dunhuang is situated at the westernmost fringe of Hexi Corridor in Gansu province,  
319 close to the eastern edge of Kumtag Desert and about 450 km in the downwind zone  
320 of Taklimakan Desert. It is an important town of the ancient Silk Road and the  
321 transportation junction to the ancient western region, central Asia and Europe, which  
322 has become a world-famous tourist city with a residential population of 200,000. The  
323 agriculture and tourism are the dominant economic industries in Dunhuang. An array  
324 of ground-based remote sensing and in situ instruments were set up during the  
325 intensive period, which sought to investigate the aerosol key properties and its

326 climatic effect on regional scale (Bi et al., 2014). This study especially aims at  
327 exploring the light scattering and absorption characteristics of mineral dust and  
328 elucidates a potential anthropogenic influence. In the following, we first introduce the  
329 site information and integrated measurements in Section 2. The primary results and  
330 discussion are described in Sect. 3. The concluding remarks are given in Sect. 4 and  
331 followed by the data availability in Sect. 5.

## 332 **2. Site and instrumentation**

### 333 **2.1. Site information**

334 SACOL's Mobile Facility (SMF) was deployed at Dunhuang farmland (40.492° N,  
335 94.955° E, 1061 m above MSL) from 1 April to 12 June 2012. The site is a tiny  
336 isolated oasis encompassed by east-west oriented Gobi desert and arid zones in  
337 northwest China, with the Mingsha Shan (Echoing-Sand Mountain, elevation: ~1650  
338 m) and Sanwei Mountain (elevation: ~1360 m) to the ~~southeast~~southwest, and the  
339 Beishan Mountain (elevation: ~2580 m) to the north (Ma et al., 2013). The underlying  
340 surface is typically covered with Gobi desert and saline-alkali land, and the principal  
341 vegetation types consist of extremely sparse Alhagi. Dunhuang farmland is an  
342 important agricultural base in Gobi desert, mainly planting hami melon and cotton.  
343 There are not any significant manmade pollution sources (e.g., large-scale industries  
344 or coal-fired power plants) around the monitoring station. The southwest-northeast  
345 oriented National Highway 215 is about 400 m away from the west of the site (Figure  
346 1a). The nearest Xihu township (with total population of 13,800) is approximately 7  
347 km to the north of Dunhuang farmland, along with some scattered villages stretching  
348 from west to east. Meanwhile, the station is located in the northeast of Dunhuang city  
349 (~45 km), at the west of Guazhou country (~70 km), and at the southwest of Liuyuan  
350 town (~80 km). In general, the major anthropogenic emission sources at Dunhuang  
351 farmland likely include coal combustion from domestic heating and cooking, mobile  
352 sources emissions from vehicle exhaust gas, and biomass burning from crop residue  
353 and traditional ritual activities, which are ordinarily considered to be a puny  
354 contribution to the mineral dust in present-day climate models. The climate pattern

355 here is characterized as extreme drought but with a moderate temperature during the  
356 whole sampling period (temperature:  $18.3\pm 8.1^{\circ}\text{C}$ , relative humidity, RH:  $21.9\pm 16.5\%$ ,  
357 mean  $\pm$  standard deviation). Thereby the dust storms frequently take place in this  
358 region from spring to early summer. Figure 1(b) shows the overall mean UV aerosol  
359 index (AI) from 1 April to 12 June 2012 obtained from the Ozone Monitoring  
360 Instrument (OMI) absorbing aerosol products (Torres et al., 2007). The AI dataset is a  
361 very good indicator for mapping the distribution of absorbing aerosols (mainly black  
362 carbon and dust). ~~The distributions of High-high AI values (>0.7) distributions~~ are  
363 well consistent with the dust-dominated geomorphological features in arid and  
364 semiarid regions (i.e., Taklimakan Desert and Gobi deserts). It is very obvious that  
365 Dunhuang (marked with a pentagram) is also situated at the primary dust belt of  
366 northwest China, as presented in Figure 1b.

## 367 2.2. Aerosol measurements

368 An aerosol integrated observing system is installed in the laboratory of SMF and  
369 utilized to continuously measure aerosol optical properties and size distribution in the  
370 field. Prior to the experiment, the in-situ aerosol instruments and broadband  
371 radiometers were newly purchased and calibrated by the manufacturers (Bi et al.,  
372 2014). Table 1 summarizes the basic specification, measured variables, and accuracy  
373 of surface-based instruments deployed at Dunhuang farmland throughout the  
374 experiment. We shall describe sequentially as below.

375 An ambient particulate monitor (Model RP1400a, Rupprecht and Patashnick  
376 Corp.) can collect the in situ mass concentration of the particulate matter with an  
377 aerodynamic diameter less than  $10\ \mu\text{m}$  ( $\text{PM}_{10}$ ) based on Tapered Element Oscillating  
378 Microbalance (TEOM) technique. The measurement range and accuracy of  $\text{PM}_{10}$   
379 concentration levels are normally  $0\text{--}5\ \text{gm}^{-3}$  and  $0.1\ \mu\text{gm}^{-3}$ , respectively. The heating  
380 temperature ( $\sim 50^{\circ}\text{C}$ ) of the sampling tube may cause a partial loss of volatile and  
381 semivolatile aerosol compounds and hence bring about a negative signal. In this study,  
382 we eliminate all the negative values of  $\text{PM}_{10}$  concentrations, which account for less  
383 than 1% of total data points.

384 An integrating nephelometer (Model 3563, TSI Inc.) is designed to simultaneously

385 measure the total scattering coefficients ( $\sigma_{sp}$ ) and hemispheric backscattering  
386 coefficients ( $\sigma_{bsp}$ ) of aerosol particles at three wavelengths of 450, 550, and 700 nm,  
387 with the  $\sigma_{sp}$  detection limits of 0.44, 0.17, and 0.26  $Mm^{-1}$  ( $1 Mm^{-1}=10^{-6} m^{-1}$ ),  
388 respectively (signal-to-noise ratio of 2) (Anderson et al., 1996). To quantify the  
389 instrument drift and improve accuracy, we periodically perform the routine calibration  
390 using air and high-purity  $CO_2$  gases. Furthermore, the truncation errors of  
391 near-forward scattering (i.e., nonideal angular effects) are corrected according to the  
392 method of Anderson and Ogren (1998). The observed ambient RH values are mostly  
393 smaller than 40% throughout the entire period. It is well-documented that RH-induced  
394 the variations in aerosol light scattering coefficients are minimized under a low  
395 sampling stream RH of 10–40% (Covert et al., 1972). In this paper, we computed the  
396 scattering Ångström exponent at 450–700 nm (SAE 450/700 nm) from  $\sigma_{sp}$  at 450 nm  
397 and  $\sigma_{sp}$  at 700 nm by utilizing a log-linear fitting algorithm. And thus  $\sigma_{sp}$  at 670 nm  
398 ( $\sigma_{sp,670}$ ) was logarithmic interpolated between  $\sigma_{sp,450}$  and  $\sigma_{sp,700}$ .

399 A multi-angle absorption photometer (MAAP Model 5012, Thermo Electron  
400 Corp.) is capable of observing the aerosol light absorption coefficient at 670 nm  
401 ( $\sigma_{ap,670}$ ) by filter based methods without requirement of post-measurement data  
402 correction or parallel-measured aerosol light-scattering coefficients (Petzold et al.,  
403 2002). The instrument detects an emitted light at 670 nm in the forward and back  
404 hemisphere of airborne aerosols deposited on a fiber filter, which is used to improve  
405 multiple scattering effects in the aerosol optical properties via a radiative transfer  
406 scheme (Petzold et al., 2002, 2005). The sample flow rate is 1000 L/h, with flow error  
407 of < 1%. We made use of a specific absorption efficiency at 670 nm of  $6.5\pm 0.5 m^2 g^{-1}$   
408 to estimate black carbon (BC) concentration from  $\sigma_{ap,670}$  as recommended by Petzold  
409 et al. (2002).

410 An Aerodynamic Particle Sizer (APS) spectrometer (Model 3321, TSI Inc.) can  
411 continuously provide the real-time, high-resolution aerosol size distribution with  
412 aerodynamic diameters from 0.5 to 20  $\mu m$  range (52 channels). When extreme dust  
413 episodes outbreak, an aerosol diluter (Model 3302A, TSI Inc.) is operated in series  
414 with APS to reduce particle concentrations in high-concentration aerosols, which

415 offers a representative sampling that meets the input requirements of the APS  
416 spectrometer. All the mentioned-above aerosol datasets were acquired at 5-minute and  
417 hourly averages, and reported for sampling volumes under standard air conditions (i.e.,  
418 1013.25 hPa and 20 °C).

### 419 **2.3. Other ground-based measurements**

420 A Micro-Pulse Lidar (Model MPL-4, Sigma Space Corp., U.S.A.) is a compact  
421 and unattended apparatus for providing continuous data information of extinction  
422 coefficient and depolarization ratio profiles of aerosols and clouds (Welton et al.,  
423 2000). The MPL-4 emits a laser beam at 527 nm wavelength from a Nd:YLF pulsed  
424 laser diode and receives the attenuated backscattering intensity and depolarized  
425 signals from aerosol particles or cloud droplets with a 30-meter vertical resolution and  
426 a 1-minute average interval. And we can acquire the accurate backscattering profile  
427 by means of a series of corrections (e.g., dead time, background signal, afterpulse,  
428 overlap, and range-corrected) according to the standard methods (Campbell et al.,  
429 2002). The detailed data acquisition and retrieval algorithms of the lidar system can  
430 be referred to the publications of Campbell et al. (2002) and Z. Huang et al. (2010).

431 A weather transmitter (Model WXT-520, Vaisala, Finland) is set up on the top of  
432 the SMF trailer and recorded the air temperature (T in °C), relative humidity (RH),  
433 ambient pressure (P, unit: hPa), wind speed and wind direction at ~~20~~-10 seconds  
434 interval. In this article, we calculated the 5-minute and hourly averages from the raw  
435 data.

436 A dozen of state-of-the-art broadband radiometers were installed in a row on a  
437 standard horizontal platform (~4 m above the surface) where the field of view was  
438 unobstructed in all directions (Bi et al., 2014). The direct normal irradiance and  
439 diffuse irradiance were independently measured by an incident pyrheliometer (Model  
440 NIP, Eppley Lab.) and by a ventilated and shaded pyranometer (Model PSP, Eppley  
441 Lab.), which were mounted on a two-axis automatic sun tracker (Model 2AP,  
442 Kipp&Zonen). The global irradiance (0.285–2.8 μm) and downward longwave  
443 irradiance (3.5–50 μm) were respectively gathered from a ventilated PSP pyranometer  
444 and a ventilated and shaded pyrgeometer (Model PIR, Eppley Lab.). All irradiance

445 quantities were stored in a Campbell data logger with 1-minute resolution.  
446 Additionally, a Total Sky Imager (Model TSI-880, YES Inc.) provides high-resolution  
447 sky pictures every one minute during the daytime, which can detect and identify the  
448 important weather conditions, such as dust storm, smoky pollution, rainy day, cloudy  
449 or cloudless days.

#### 450 **2.4. MERRA reanalysis products**

451 The MERRA (Modern-Era Retrospective Analysis for Research and Applications)  
452 reanalysis assimilates a variety of conventional observations (i.e., temperature,  
453 pressure, height, wind components) from surface weather stations, balloons, aircraft,  
454 ships, buoys, and satellites from 1980 to the present, which is primarily committed to  
455 improve upon the hydrologic cycle and energy budget for the science community  
456 (Rienecker et al., 2011). In this paper, we took advantage of the 6-hourly average  
457 wind fields at 500 hPa and 850 hPa levels from the MERRA reanalysis products.

### 458 **3. Results and discussion**

#### 459 **3.1 Aerosol optical properties**

460 The aerosol single-scattering albedo (SSA) at 670 nm is defined as the ratio of the  
461 light scattering coefficient ( $\sigma_{sp,670}$ ) to the total extinction coefficient (the sum of  $\sigma_{sp,670}$   
462 and  $\sigma_{ap,670}$ ). The SSA reflects the absorptive ability of aerosol particle and is a key  
463 quantity in determining the sign (warming or cooling) of aerosol radiative forcing for  
464 a certain underlying surface (Hansen et al., 1997; Ramanathan et al., 2001).

465 Figure 2 delineates the time series of hourly average  $PM_{10}$  mass concentration,  
466 aerosol optical properties and size distribution at Dunhuang farmland during the  
467 whole period. The overall mean, standard deviation, median, and different percentiles  
468 of aerosol optical properties are also tabulated in Table 2. Aerosol optical features  
469 exhibit dramatic day-to-day variations at Dunhuang. It is apparent that aerosol  
470 loadings in April and early May are systematically higher than that in late May and  
471 June, which agrees well with the results of columnar aerosol optical depths derived  
472 from sky radiometer (Bi et al., 2014). This is chiefly attributed to the invading mineral  
473 particulates from the frequent occurrences of intense dust storms in spring season.



474 | The highly unstable synoptic cyclones (i.e., Mongolian cyclones) are regularly  
475 | hovering about the northern China and Mongolia in springtime, which trigger  
476 | high-frequency strong surface winds (Sun et al., 2001; Shao et al., 2011). The rising  
477 | temperature in this season leads to the melting of frozen soil and snow cover, leaving  
478 | behind a loose land surface and abundant bare soil sources, therefore affords a  
479 | favorable condition for dust storms. In addition, the contributions of local dust  
480 | emissions couldn't be ignored. We have clearly recorded that there were numerous  
481 | agricultural cultivated operations (e.g., land planning, plowing, and disking)  
482 | throughout the Dunhuang farmland district from 1 April to 10 May, which produced a  
483 | great amount of agricultural soil particles under strong winds, and thus had a  
484 | significant superimposed effect on elevated dust loading in the source and downwind  
485 | regions prior to the growing season. [Figure S1 also presents visual photos of a variety](#)  
486 | [of agricultural cultivations in Dunhuang farmland before the planting period, which](#)  
487 | [supplies direct and powerful evidences for supporting our results.](#) Those dust aerosols  
488 | originated from disturbed soils induced by human activities are interpreted as  
489 | anthropogenic dust (Tegen and Fung, 1995). Recently, some investigators estimated  
490 | that anthropogenic dust could account for approximately 25% of the global dust load  
491 | (Ginoux et al., 2012; Huang et al., 2015), and more than 53% of the anthropogenic  
492 | sources mostly came from semi-arid and semi-wet zones (Huang et al., 2015; Guan et  
493 | al., 2016). Nonetheless, it still remains a challenging task to distinguish between the  
494 | natural and anthropogenic fractions of mineral dust by employing a onefold  
495 | technology, for instance, laboratory analysis, in situ measurements, model simulations,  
496 | active and passive remote sensing methods (e.g., multichannel lidar, sun/sky  
497 | radiometer), which should be combined together (Bi et al., 2016). The overall mean  
498 |  $PM_{10}$  concentration was  $113 \pm 169 \mu g m^{-3}$  (mean  $\pm$  standard deviation), which is  $\sim 39\%$   
499 | lower than the  $184.1 \pm 212 \mu g m^{-3}$  average level in Dunhuang ( $40.1^\circ N$ ,  $94.6^\circ E$ , 1139  
500 | m) during the spring of 2004 (Yan, 2007), and  $\sim 26\%$  smaller than the value of  
501 |  $153 \pm 230 \mu g m^{-3}$  measured at Zhangye ( $39.082^\circ N$ ,  $100.276^\circ E$ , 1460 m) during spring  
502 | of 2008 (Li et al., 2010). Wang et al. (2015) obtained a total average  $PM_{10}$   
503 | concentration of  $172 \pm 180 \mu g m^{-3}$  at SACOL during late spring of 2007 (from 25 April

504 to 25 June). And the mean  $PM_{10}$  levels at Hunshan Dake sandland in northern China  
505 during spring of 2001 varied between 226 and 522  $\mu\text{gm}^{-3}$  (Cheng et al., 2005).

506 The hourly average aerosol light scattering coefficient at 670 nm ( $\sigma_{\text{sp},670}$ ) was  
507  $53.3 \pm 74.8 \text{ Mm}^{-1}$ . The big standard deviations of  $PM_{10}$  and  $\sigma_{\text{sp}}$  are possibly associated  
508 with the injection of dust particles during the intense dust storms. Our result was  
509 about a factor of 3 lower than the  $\sigma_{\text{sp}}$  at 500 nm in mentioned-above other sites over  
510 northern China (i.e.,  $126 \pm 90 \text{ Mm}^{-1}$  for Dunhuang,  $159 \pm 191 \text{ Mm}^{-1}$  for Zhangye,  
511  $164 \pm 89 \text{ Mm}^{-1}$  for SACOL). Despite relatively small magnitude, the aerosol light  
512 absorption coefficient at 670 nm ( $\sigma_{\text{ap},670}$ ) also presented pronounced variations, with  
513 an average value and a maximum of  $3.2 \pm 2.4 \text{ Mm}^{-1}$  and  $25.0 \text{ Mm}^{-1}$ , respectively. This  
514 result was a factor of 2 smaller than Yulin ( $6 \pm 11 \text{ Mm}^{-1}$ ) nearby Mu Us desert in  
515 northwest China (Xu et al., 2004), and a factor of 5~7 far less than that at Shangdianzi  
516 rural site ( $17.5 \pm 13.4 \text{ Mm}^{-1}$ ) in northern China (Yan et al., 2008) and Lin'an site ( $\sim 23$   
517  $\text{Mm}^{-1}$ ) in southern China (Xu et al., 2002). The mean light scattering and absorption  
518 coefficients in this study are comparable to the background levels ( $\sim 46.9 \pm 16.9$  and  
519  $2.5 \pm 1.1 \text{ Mm}^{-1}$ ) in Southern Great Plain of U.S.A (Delene and Ogren, 2002). This  
520 suggests that extremely low levels of light absorption and scattering substances are  
521 widely distributed throughout the Dunhuang region during the spring of 2012.  
522 Therefore, a little perturbation stemmed from human activities (e.g., agricultural  
523 cultivation, coal combustion from domestic heating and cooking, and biomass burning)  
524 would undoubtedly exert a considerable impact on the light absorption property.

525 A few of strong dust episodes (4, 21–22, and 30 April, 1–3, 8–11, and 20 May, 4  
526 and 10 June, corresponding to DOY 95, 112–113, 121, 122–125, 129–132, 141, 156,  
527 and 162) could remarkably elevate the hourly average values of  $PM_{10}$ ,  $\sigma_{\text{sp}}$ ,  $\sigma_{\text{ap}}$ , and  
528 aerosol size distribution (see Figure 2). During these dust events, the hourly  $PM_{10}$   
529 concentrations generally exceeded 1000  $\mu\text{gm}^{-3}$  and even approached 2000  $\mu\text{gm}^{-3}$ ,  
530 which were tenfold greater than the overall mean level. The hourly  $\sigma_{\text{sp}}$  were more  
531 than  $400 \text{ Mm}^{-1}$  or even close to  $800 \text{ Mm}^{-1}$ , and the corresponding  $\sigma_{\text{ap}}$  varied between  
532  $10 \text{ Mm}^{-1}$  and  $25 \text{ Mm}^{-1}$ . Moreover, the peak values of aerosol number size distribution  
533 concentrated in the particle diameters of 1–3  $\mu\text{m}$ , which was consonant with the result

534 from remote sensing (Bi et al., 2014, 2016).

535 Figure 3 depicts the time evolutions of MPL normalized relative backscatter and  
536 depolarization ratio at Dunhuang farmland from 1 April to 12 June 2012. The  
537 depolarization ratio ( $\delta$ ) is a useful indication to discriminate between spherical  
538 particles ( $\delta$  of  $\sim 0$ – $0.1$ ) and nonspherical particles (mainly dust aerosol,  $\delta > 0.2$ ), since  
539 it is very sensitive to the nonsphericity of scattering particle (Kobayashi et al., 1985;  
540 Murayama et al., 1999; Shimizu et al., 2004; Huang et al., 2015). From Figure 3, we  
541 can distinctly see that there was always a dense dust layer appeared at a height below  
542 ~~2 to~~ 4 km during the whole experiment, with the peak value centered on 1.0–1.5 km,  
543 which was ~~within~~ above the planetary boundary layer (PBL). And the  $\delta$  values  
544 commonly reached above 0.3 ( $> \sim 0.3$ – $0.5$ ) during the heavy dust events and varied  
545 between 0 and 0.1 under clear-sky conditions (e.g., 6–7 April, 14–15 and 29 May, 9  
546 June).

### 547 3.2 Diurnal variations

548 Figure 4 illustrates the diurnal variations of wind vector ( $\text{ms}^{-1}$ ), air temperature ( $T$   
549 in  $^{\circ}\text{C}$ ), RH (%),  $\text{PM}_{10}$  ( $\mu\text{gm}^{-3}$ ),  $\sigma_{\text{sp},670}$  ( $\text{Mm}^{-1}$ ),  $\sigma_{\text{ap},670}$  ( $\text{Mm}^{-1}$ ), aerosol number size  
550 distribution ( $\text{dN}/\text{dlogD}$  in  $\text{cm}^{-3}$ ), SAE at 450–700 nm, and SSA at 670 nm in  
551 Dunhuang farmland from 1 April to 12 June 2012. Note that the APS spectrometer  
552 was operated from 30 May to 12 June. A discernible wind vector was ~~showed~~ shown  
553 in the diurnal variation, in other words, strong southwest wind and south wind  
554 dominated in the daytime, from 11:00 to 24:00 LT (local time), and transformed into  
555 the weak northeast wind prevailed from the midnight to the following morning of  
556 10:00 LT. The prominent phenomenon can be roughly interpreted by classical  
557 mountain-valley wind circulation, which was primarily generated by the diurnal  
558 differences of temperature between the mountain slope and the valley floor. During  
559 the daytime, the huge Beishan Mountain slope heats up by the solar radiation more  
560 rapidly than the valley floor, which causes convection above the mountain slope. The  
561 compensating airflow is consequently directed toward the mountain slope, inducing  
562 upslope southerly wind, or the valley wind, which usually peaks near midday and  
563 gradually disappears after sunset. Conversely, at night, radiative cooling of the

564 mountain slope is more quickly than the valley floor, inducing the mountain wind,  
565 which generally reaches maximum strength just before sunrise (Arya, 1999).  
566 Throughout the experiment, air temperature displayed a large diurnal variation (with  
567 the diurnal difference of  $\delta T \sim 26$  °C) and RH always kept below 40% for the whole day.  
568 It is very clear that the minimal T and maximal RH arose at around 06:00–07:00 LT,  
569 and the maximal T and minimal RH occurred at about 16:00 LT, which represented an  
570 energetic vertical turbulent motion in daytime and a stable radiative temperature  
571 inversion during nighttime.

572 The aerosol optical parameters also exhibited striking diurnal variations, which  
573 were closely related to the local meteorological elements. During the daytime  
574 (10:00–18:00 LT), the  $PM_{10}$  concentration remained high level ( $\sim 57$ – $65$   $\mu\text{gm}^{-3}$ ) and  
575 increased sharply from 19:00 LT and reached a maximum of  $84.2$   $\mu\text{gm}^{-3}$  at 20:00 LT.  
576 The  $PM_{10}$  began to decrease from 21:00 LT to the next morning. A low level ( $\sim 40$ – $46$   
577  $\mu\text{gm}^{-3}$ ) kept in the midnight (00:00–05:00 LT) and rose gradually from 06:00 LT and  
578 attained a secondary peak value of  $55.7$   $\mu\text{gm}^{-3}$  at 07:00 LT. The aerosol light  
579 scattering ( $\sigma_{\text{sp},670}$ ) presented a similar pattern with  $PM_{10}$ , but the maximal value ( $\sim 42$   
580  $\text{Mm}^{-1}$ ) appeared at 13:00 LT, with the other two secondary peak values occurred at  
581 20:00 ( $\sim 34.1$   $\text{Mm}^{-1}$ ) and 07:00 LT ( $\sim 27.3$   $\text{Mm}^{-1}$ ). The high levels of  $PM_{10}$  and  $\sigma_{\text{sp}}$   
582 during the daytime were primarily attributable to strong south wind from Gobi region  
583 and local dust emissions. By contrast, aerosol light absorption coefficient ( $\sigma_{\text{ap},670}$ )  
584 showed a more pronounced diurnal feature, which was well proved to be majorly  
585 controlled by anthropogenic emissions (Li et al., 2010). The diurnal  $\sigma_{\text{ap}}$  always stayed  
586 at a low level ( $\sim 2.0$   $\text{Mm}^{-1}$ ) from 13:00–18:00 LT, and also reached a maximum of  $3.3$   
587  $\text{Mm}^{-1}$  at 20:00 LT. Subsequently,  $\sigma_{\text{ap}}$  dramatically reduced from midnight and  
588 preserved at a low value of about  $2.2$   $\text{Mm}^{-1}$  from 02:00–04:00 LT, and remained a  
589 steadily high level of  $\sim 2.7$ – $2.9$   $\text{Mm}^{-1}$  from 05:00–10:00 LT. It was probably explained  
590 as follows. The influences of local anthropogenic pollutants were commonly small in  
591 the afternoon, because the strong southerly wind from Gobi deserts and powerful  
592 daytime vertical convection mixing efficiently dilute local air pollutants. Whereas  
593 weak northeast wind and stable temperature inversion at night facilitate the

594 accumulation of pollutants within the PBL, hence nighttime levels were normally  
595 larger. Increasing human activities (e.g., domestic cooking, traffic emissions for  
596 transportation and agriculture) in the early morning might also be responsible for the  
597 morning peaks in the aerosol absorption coefficient. The  $\sigma_{ap}$  maximum at 20:00 LT  
598 was presumably influenced by the mixture of mineral dust and anthropogenic  
599 pollutants. This conclusion could be partly supported by the diurnal variation of SAE  
600 at 450–700 nm (Figure 4), which showed high SAE values ( $\sim 0.5$ – $0.6$ ) appeared at  
601 02:00–10:00 LT and low SAE ( $\sim 0.2$ – $0.3$ ) occurred on 13:00–22:00 LT. Generally,  
602 large SAE around 0.6 represents small particles (e.g., urban-polluted aerosol or soot)  
603 and low SAE less than 0.3 or negative value corresponds to coarse-dominated large  
604 size particles (e.g., dust or sea salt) (Anderson et al., 2003).

605 Furthermore, aerosol number size distribution exhibited a noticeable supermicron  
606 particles dominated in the entire day, probably linked to the predominant dust aerosol  
607 in daytime and local anthropogenic emissions at nighttime. In this study, we  
608 postulated that the aerosol light extinction at shortwave waveband is completely  
609 caused by those particles with aerodynamic diameters of 10  $\mu\text{m}$  or less. And the mass  
610 scattering efficiency is designated as the ratio of  $\sigma_{sp}$  to  $\text{PM}_{10}$  concentration. Therefore,  
611 the mass scattering efficiency for  $\text{PM}_{10}$  aerosols was about  $0.67 \text{ m}^2\text{g}^{-1}$  in the afternoon  
612 and  $\sim 0.77 \text{ m}^2\text{g}^{-1}$  in the morning ( $\sim 0.25$  for heavy dust events, and  $\sim 0.70$  for the whole  
613 period). Our results were slightly less than  $\sim 1.05 \text{ m}^2\text{g}^{-1}$  in Dunhuang during spring of  
614 | 2004 (Yan, 2007). **SimilarlyLikewise**, the mass absorption efficiency was  $\sim 0.017$   
615  $\text{m}^2\text{g}^{-1}$  under heavy dust episodes and  $\sim 0.08 \text{ m}^2\text{g}^{-1}$  in the morning, which was  
616 coincident with the laboratory analytical result of natural desert aerosol at 660 nm  
617 ( $\sim 0.01$ – $0.02 \text{ m}^2\text{g}^{-1}$ ) in Ulan Buh desert ( $39^\circ 26' \text{N}$ ,  $105^\circ 40' \text{E}$ ) of northern China (Alfaro  
618 et al., 2004). These diurnal variations of the mass scattering and absorption  
619 efficiencies likely reflect the changes in aerosol chemical composition. The SSA at  
620 670 nm displayed distinct differences between daytime and nighttime (Figure 4), and  
621 the two minimal values at 07:00 LT ( $\sim 0.90$ ) and 20:00 LT ( $\sim 0.921$ ) were consistent  
622 with the aforementioned  $\sigma_{ap,670}$  diurnal feature. The peak values of SSA ( $0.945 \pm 0.04$ )  
623 for dominant dust particles in the afternoon agreed well with other field campaigns in

624 Zhangye ( $0.95\pm 0.02$ , Li et al., 2010) and Yulin ( $0.95\pm 0.04$ , Xu et al., 2004). The daily  
625 low SSA ( $0.90\text{--}0.92$ ) or overall mean of  $0.913\pm 0.055$  at Dunhuang was still bigger  
626 than that in both urban ( $0.81$ , Bergin et al., 2001) and rural regions ( $0.81\text{--}0.85$ , Li et  
627 al., 2007) adjacent to Beijing, presumably ascribed to dust particles at night. Yan et al.  
628 (2008) conducted two-year long field measurements at Shangdianzi Global  
629 Atmosphere Watch (GAW) rural site in northern China ( $\sim 150$  km from Beijing) and  
630 estimated a mean SSA of  $0.88\pm 0.05$ , but their data contained summer when aerosol  
631 scattering coefficients may be strengthened by hygroscopic growth and secondary  
632 chemical process.

633 The wind rose plots give a further insight into the linkages between the  
634 meteorological factors and pollutants, as described in Figure 5. In the morning  
635 (06:00–09:00 LT), a marked northeast wind was prevalent and wind speed was mostly  
636 less than  $4\text{ ms}^{-1}$ , which revealed that emissions were primarily descended from nearby  
637 farmlands and rural residences (Figure 5a). Although a prominent northwest wind  
638 mainly occurred in the evening hours (19:00–22:00 LT), the east wind and southwest  
639 wind also appeared, which indicated that anthropogenic pollutions came from both  
640 local sources and a relatively large region along the valley (Figure 5b). And Figure 5c  
641 showed the predominant winds were northeast and southwest winds in Dunhuang area,  
642 with the maximal hourly-averaged wind speed exceeding  $10\text{ ms}^{-1}$ . It was very distinct  
643 that the southwest and northwest winds created higher levels of  $\text{PM}_{10}$  mass  
644 concentration ( $>250\text{ }\mu\text{g m}^{-3}$ ), aerosol light scattering coefficient ( $\sigma_{\text{sp}} >150\text{ Mm}^{-1}$ ) and  
645 absorption coefficient ( $\sigma_{\text{ap}} >8\text{ Mm}^{-1}$ ), whereas northeast wind generated slightly  
646 smaller concentrations of  $\text{PM}_{10}$  ( $\sim 50\text{--}100\text{ }\mu\text{g m}^{-3}$ ),  $\sigma_{\text{sp}}$  ( $\sim 30\text{--}60\text{ Mm}^{-1}$ ) and  $\sigma_{\text{ap}}$  ( $\sim 2\text{--}4$   
647  $\text{Mm}^{-1}$ ). This was possibly implied that southwest and northwest winds may bring  
648 about dust particles and northeast wind may transport the air pollutants.

### 649 **3.3 Local anthropogenic emission sources**

650 As mentioned above, crop residue burning and agricultural cultivated operations  
651 before the growing season could produce local emission source proximity to the study  
652 area. And sporadic straw burning was indeed to happen throughout the Dunhuang  
653 farmland from 1 April to 10 May 2012, which was the major source of black carbon

654 surrounding the site. To clarify the potential anthropogenic influence on aerosol  
655 optical properties in desert region, we investigated a typical biomass burning event.

656 Figure 6 outlines the time series of 5-minute average wind vector ( $\text{ms}^{-1}$ ),  $\text{PM}_{10}$   
657 ( $\mu\text{gm}^{-3}$ ),  $\sigma_{\text{sp}}$  at 450, 550, and 700 nm ( $\text{Mm}^{-1}$ ), SAE (450–550, 550–700, and 450–700  
658 nm),  $\sigma_{\text{ap},670}$  ( $\text{Mm}^{-1}$ ), and SSA at 670 nm during a typical Tomb-sweeping Day on 4  
659 April 2012. Tomb-sweeping Day is a Chinese traditional festival for sacrifice rites, in  
660 commemoration of the dead ancestors. To pay homage to loved ones, the people  
661 burned a lot of joss sticks, candles, and paper offerings, and set off firecrackers in that  
662 day throughout the China, which would emit a great amount of air pollutants, such as,  
663 biomass burning aerosol, sulfur dioxide, organic matter, and fugitive dust. From  
664 Figure 6a, slight and variable winds (with wind speed  $<4 \text{ ms}^{-1}$ ) mainly came from  
665 northeasterly from 00:00 to 12:00 LT, and abruptly changed into weak southeast wind  
666 and south wind, finally, gradually intensified southwest wind ( $>10 \text{ ms}^{-1}$ ) were  
667 predominant and triggered a severe dust storm from 15:00 LT to the midnight. Prior to  
668 the occurrence of dust episode, the aerosol optical characteristics varied stably, but a  
669 moderate increase was evident during 08:00 to 10:00 LT. For instance,  $\text{PM}_{10}$   
670 concentration gradually increased from background level  $\sim 30 \mu\text{gm}^{-3}$  to a maximum of  
671  $62.5 \mu\text{gm}^{-3}$  at about 09:00 LT,  $\sigma_{\text{sp},550}$  from  $\sim 15 \text{ Mm}^{-1}$  to  $49.6 \text{ Mm}^{-1}$ , and  $\sigma_{\text{ap},670}$  from  
672  $\sim 2.0 \text{ Mm}^{-1}$  to  $4.75 \text{ Mm}^{-1}$ . It is ascribed to the contribution of biomass burning in the  
673 process of ritual activities during Tomb-sweeping Day. The SAE value at 450–700 nm  
674 remained invariant ( $\sim 0.50$ ) before 08:00 LT and sharply rose to a maximal value of  
675 0.87 at 09:00 LT, afterwards gently reduced to around 0.4, which indicated that the  
676 fine-mode particles (i.e., black carbon or soot) were dominated from 08:00 to 10:00  
677 LT. And the SAEs at various wavelengths systematically decreased from 0.4 at 15:00  
678 LT to -0.25 at midnight, suggesting the dust-dominant coarse-mode particles were  
679 prevailed. Meanwhile, the lidar depolarization ratio ( $\delta$ ) also further verified the  
680 existence of small size soot particle. The  $\delta$  value preserved steadily at 0.15–0.20  
681 during 08:00 to 10:00 LT, and rapidly attained above 0.3 from 15:00 LT and even  
682 approached 0.50 at intense dust storm (see Fig. 3). The diurnal variation of  $\text{SSA}_{670}$   
683 showed a more prominent feature, as illustrated in Figure 6f. The  $\text{SSA}_{670}$  values kept

684 between 0.88 and 0.92 during 00:00 to 07:00 LT, and dramatically reduced to a  
685 minimum of ~0.83 at 08:30–09:00 LT, then rose to 0.925, confirming the very striking  
686 impacts by light absorbing substances. After 15:00 LT, the  $SSA_{670}$  gradually increased  
687 and reached up to about 0.96 during dust storms occurred. Bi et al. (2014) have  
688 demonstrated that dust aerosols shortwave radiative forcing (ARF) at the top of the  
689 atmosphere (TOA) was warming effect when  $SSA_{500}$  was less than 0.85, but was  
690 cooling effect when  $SSA_{500}$  was greater than 0.85 for Dunhuang Gobi desert area with  
691 high surface albedo. Thereby such significant anthropogenic influence would clearly  
692 modify the microphysical and chemical properties of dust aerosols and eventually  
693 exert remarkable impacts on environmental quality and climatic forcing of dust  
694 particle on both local and regional scales.

### 695 **3.4 Dust cases study**

696 In this section, we particularly explored the absorptive and optical characteristics  
697 of mineral dust during several typical dust cases and discussed its influence on Earth's  
698 radiation balance. Figure 7 provides the wind fields at 500 hPa and 850 hPa levels  
699 during three heavy dust events, based on MERRA reanalysis products. Note that  
700 Dunhuang farmland is marked with a red pentagram and the white areas at 850 hPa  
701 represent the missing values. It is evident that East Asian region was governed by the  
702 powerful and stable westerlies at 500 hPa height on 30 April and 1 May 2012,  
703 whereas two very strong synoptic cyclones at 500 hPa upper atmosphere hovered  
704 about the Mongolia and Kazakhstan respectively on 10 June 2012, matching up with  
705 corresponding cyclone systems appeared at the 850 hPa level. Although there were  
706 missing data in most northwest China, extremely intense northeast wind and east wind  
707 ( $> 10 \text{ ms}^{-1}$ ) at 850 hPa level were prevailed over the northern territory of Xinjiang  
708 Uygur Autonomous Region during the selected dust storms, where was close to the  
709 Dunhuang site. This could be well confirmed by the simultaneous observations of  
710 wind speed and wind direction nearby the surface at Dunhuang farmland, as  
711 delineated in Figure 8(a). The measured strong northeast and east winds were always  
712 dominated in Dunhuang and 5-min average wind speed attained above  $10 \text{ ms}^{-1}$  during  
713 intense dust episodes. The selected three dust processes regularly lasted for several



714 hours during daytime (e.g., from 10:00 to 18:00 LT) and the dust event on 1 April  
715 could be persistent to the midnight, which contributed massive dust particles into the  
716 atmosphere.

717 There were no measurements of aerosol scattering coefficient ( $\sigma_{sp}$ ) on 10 June due  
718 to equipment failure. From Figure 8, we could know that  $PM_{10}$  concentrations usually  
719 exceeded  $400 \mu\text{gm}^{-3}$  and even reached up to  $1000 \mu\text{gm}^{-3}$  during the heavy dust storms,  
720 and corresponding  $\sigma_{sp,550}$  and  $\sigma_{ap,670}$  values were generally more than  $100 \text{Mm}^{-1}$  and 5  
721  $\text{Mm}^{-1}$ , respectively, or approached  $350 \text{Mm}^{-1}$  and  $15 \text{Mm}^{-1}$  in our cases. It is worthy  
722 note that even though pure dust aerosol possesses relatively low light-absorption  
723 ability (with mass absorption efficiency at 660 nm of  $\sim 0.01\text{--}0.02 \text{m}^2\text{g}^{-1}$ ), the injection  
724 of plentiful mineral particles from dust episodes led to considerably high values of  
725  $\sigma_{ap,670}$ . And the SAEs at diverse wavelengths commonly kept at 0.50 or more during  
726 non-dust conditions, while corresponding values dramatically reduced to  $-0.25\text{--}0$   
727 under heavy dust cases, which is taken for granted. The  $SSA_{670}$  also exhibited  
728 apparent diurnal variations in Figure 8(f). The  $SSA_{670}$  values regularly preserved  
729 between 0.88 and 0.92 at nighttime or non-dust weather, and gradually increased to a  
730 maximum of  $\sim 0.96\text{--}0.98$  during strong dust processes, which were close to the  
731 measured value of  $\sim 0.97\text{--}0.99$  for nearly pure Asian dust particles (Anderson et al.,  
732 2003; Bi et al., 2016). These abundant mineral particles in desert source regions were  
733 very likely mixed with local air pollutants especially at night, when the anthropogenic  
734 pollutions favorably built up within the PBL. Moreover, airborne dust particles  
735 | ordinarily traveled long distances to downstream areas via ~~mesoscale~~-synoptic  
736 cyclones, which would deteriorate the ambient air quality and affected atmospheric  
737 chemistry and climate change on regional scale.

738 Figure 9 describes the column-integrated aerosol optical depth (AOD) at five  
739 wavelengths (400, 500, 675, 870, and 1018 nm) versus Ångström exponent ( $\alpha$ ) at  
740 400–870 nm on two completely clear-sky days (14 May and 9 June) and two typical  
741 dusty days (30 April and 10 June), which were acquired from sky radiometer (Model  
742 POM-01, PREDE Co. Ltd.). The sky radiometer can measure the direct solar  
743 irradiances and sky diffuse radiances at narrow spectral wavebands during daytime

744 with 10-minute interval. And the columnar aerosol optical properties under cloudless  
745 conditions were retrieved from sophisticated inversion algorithms (Nakajima et al.,  
746 1996). Note that the cloud contaminated datasets have been eliminated by means of a  
747 series of cloud screening procedures developed by Khatri and Takamura (2009). From  
748 Figure 9, all AOD values under clear-sky days kept very stable variations throughout  
749 the day and ranged from 0.02 to 0.12, which were comparable to the clean  
750 background levels in the central Tibetan Plateau (Xia et al., 2011) and Badain Jaran  
751 Desert (Bi et al., 2013). And the corresponding Ångström exponent  $\alpha$  on 14 May and  
752 9 June were greater than 0.6, indicating extremely low aerosol loading. In contrast,  
753 the AODs under dust events (30 April and 10 June) displayed pronounced diurnal  
754 variations and all AOD values were larger than 0.30 (with maximum of 0.60), and  $\alpha$   
755 varied between 0.10 and 0.25, representing high dust concentration levels. These  
756 elevated dust particles in the atmosphere would readjust the energy distributions of  
757 solar radiative fluxes at the surface.

758 Based on aforementioned measurements of total sky imager, micro-pulse lidar and  
759 sky radiometer, we identified three completely clear-sky days (14 May, 29 May, and 9  
760 June) and two “clean” dusty days (30 April and 10 June). The “clean” dusty days in  
761 this study were denoted as the dust storms weather without the influence of clouds.  
762 This afforded us a good opportunity to elucidate the potential impacts of dust events  
763 on radiation balance at the ground. Figure 10 draws the 1-minute average solar direct  
764 normal radiation, sky diffuse radiation, total shortwave radiation, and downward  
765 long-wave radiation fluxes under the selected five days, which were derived from the  
766 high-precision broadband radiometers as described in section 2.3. All radiative  
767 quantities presented smooth diurnal variations under clear-sky cases (14 May, 29 May,  
768 and 9 June). The airborne dust particles impeded the sunlight to the ground through  
769 scattering and absorbing solar radiation, for instance, they could significantly reduced  
770 the surface direct radiative fluxes in daytime about 200–350  $\text{Wm}^{-2}$  (Figure 10a),  
771 whereas considerably increased the surface diffuse radiative fluxes up to ~150–300  
772  $\text{Wm}^{-2}$  (Figure 10b). As a result, the overall attenuation effect on total shortwave  
773 radiative fluxes varied between –150 and –50  $\text{Wm}^{-2}$ . The incoming solar energy

774 absorbed by dust particles would heat the atmospheric dust layer (Bi et al., 2014) that  
775 likely played a profound role in the structure of atmospheric boundary layer  
776 ~~structure~~ and cloud microphysical process (J. Huang et al., 2006, 2010; Li et al., 2016).  
777 The downward longwave radiation (DLW) at the surface was majorly reliant on the  
778 clouds, water vapor, CO<sub>2</sub>, and other greenhouse gases (Wang and Dickinson, 2013).  
779 In general, the presence of clouds in the atmosphere would fluctuate drastically the  
780 diurnal variation of DLW. And the smooth changes of DLW under both clear-sky and  
781 dusty days in Figure 10d revealed the robustness of the cloud screening method used  
782 in this paper. Figure 10d displays that the DLW values under dusty cases were always  
783 greater than that in clear-sky cases, with the total average differences of +40~+60  
784 Wm<sup>-2</sup>. The warming dust layer could enhance the surface DLW, hence the dust  
785 particles should contribute a few-large percentages to the increased DLW, but not all.  
786 This is because the potential greenhouse-gaseswater vapor in the atmosphere could  
787 substantially affect the DLW variations. For instance, the DLW on 9 June were  
788 distinctly lager-larger than that in other cloudless cases (i.e., 14 and 29 May) and the  
789 dusty case of 30 April. It is partly attributable to the higher RH values on 9 June than  
790 that in other days, as shown in Figure S2.

#### 791 4. Concluding remarks

792 In this article, we surveyed the optical features and size distribution of dust  
793 aerosol in a Gobi farmland region of northwest China from 1 April to 12 June 2012,  
794 and uncovered a potential anthropogenic influence. The overall average PM<sub>10</sub> mass  
795 concentration, light scattering coefficient ( $\sigma_{sp,670}$ ), absorption coefficient ( $\sigma_{ap,670}$ ), and  
796 single-scattering albedo (SSA<sub>670</sub>) throughout the experiment were  $113\pm 169 \mu\text{gm}^{-3}$ ,  
797  $53.3\pm 74.8 \text{ Mm}^{-1}$ ,  $3.2\pm 2.4 \text{ Mm}^{-1}$ , and  $0.913\pm 0.05$ , which were comparable to the  
798 background levels in southern United States, but lower than that in the eastern and  
799 other northwestern China. Frequent dust storms could markedly elevate dust loading  
800 and dominated the temporal evolution of airborne aerosol in Dunhuang region. The  
801 hourly average PM<sub>10</sub>,  $\sigma_{sp,670}$ , and  $\sigma_{ap,670}$  reached up to  $2000 \mu\text{gm}^{-3}$ ,  $800 \text{ Mm}^{-1}$ , and  $25$   
802  $\text{Mm}^{-1}$  during the severe dust events that were tenfold greater than the total mean

803 values, along with the particle size concentrated in diameters of 1–3  $\mu\text{m}$ . Meanwhile,  
804 the correspondingly high  $\text{SSA}_{670}$  ( $\sim 0.96\text{--}0.98$ ) and depolarization ratio ( $\delta$  of  $\sim 0.3\text{--}0.5$ ),  
805 and low SAE ( $-0.25\sim 0$ ) values adequately verified the presence of coarse-mode  
806 mineral dust, resulting in significantly reducing the solar direct radiation ( $\sim 200\text{--}350$   
807  $\text{Wm}^{-2}$ ) and increasing diffuse radiation ( $\sim 150\text{--}300 \text{Wm}^{-2}$ ) at the surface, and hence  
808 affecting the regional climate.

809 Owing to relatively low aerosol levels observed in Dunhuang, any slightly  
810 anthropogenic perturbation would induce a substantial influence on the aerosol  
811 physicochemical property. The so-called anthropogenic dust produced by agricultural  
812 cultivating operations (e.g., land planning, plowing, and disking) brought a significant  
813 superimposed effect on high dust concentrations in Dunhuang farmland prior to the  
814 growing season, when the underlying surface was primarily covered with bare soils.  
815 This to some extent could be interpreted the drastic changes of aerosol loadings in  
816 April and early May. In contrast, the local pollutant emissions mainly affected the  
817 absorptive characteristics of dust aerosol especially at night, when the anthropogenic  
818 pollutants favorably accumulated within the PBL and likely mixed with abundant  
819 mineral dust in the atmosphere. Therefore, the diurnal variations of  $\sigma_{\text{ap},670}$  and  $\text{SSA}_{670}$   
820 exhibited prominent features, both of which have got two peak values at night and in  
821 the early morning. For instance,  $\sim 3.3 \text{Mm}^{-1}$  at 20:00 LT and  $\sim 2.9 \text{Mm}^{-1}$  at 08:00 LT  
822 for  $\sigma_{\text{ap},670}$  were much more than the low level of  $\sim 2.0 \text{Mm}^{-1}$  in the afternoon, which  
823 was attributed to the influence of anthropogenic emissions. And the mean  $\text{SSA}_{670}$  of  
824 predominant dust particles in the afternoon (13:00–18:00 LT) was  $0.945\pm 0.04$  that  
825 was evidently greater than the mixed dust-pollutants dominated  $\text{SSA}_{670}$  of  $\sim 0.90$  at  
826 07:00 LT and  $\sim 0.92$  at 20:00 LT.

827 | The findings of this study directly demonstrated that mineral dust in Dunhuang  
828 farmland was substantially affected by anthropogenic pollutants, which would help to  
829 promote a further insight into the interaction among dust aerosol, atmospheric  
830 chemistry, and regional climate in desert source region. However, the potentially  
831 anthropogenic influences on dust aerosol in Dunhuang showed far smaller than that  
832 measured in eastern China, which was expected for the remote desert areas with

833 sparsely population and lesser human activities. Recently, Huang et al. (2016)  
834 indicated that most of the drylands in the world were fragile and susceptible to climate  
835 change and human activities and would be subject to the acceleration of drought  
836 expansion by the end of twenty-first century. Under the possible scenario, it is very  
837 critical to make clear the relative contributions of natural and anthropogenic forcing  
838 factors on global climate change, such as, natural dust and anthropogenic dust, which  
839 calls for further investigating through a lot more observations and technologies.

## 840 **5. Data availability**

841 All ground-based aerosol datasets used in this paper are available via contacting  
842 Jianrong Bi (bijr@lzu.edu.cn).

843

844 *Acknowledgements.* This work was jointly supported by the Foundation for Innovative  
845 Research Groups of the National Natural Science Foundation of China (41521004), the National  
846 Natural Science Foundation of China (41575015 and 41405113), the Fundamental Research Funds  
847 for the Central Universities lzujbky-2015-4 and lzujbky-2016-k01, and the China 111 Project (No.  
848 B 13045). The authors would like to express special thanks to David S. Covert for guiding the  
849 in-situ aerosol measurements. We thank the OMI and MERRA teams for supplying the satellite  
850 data and reanalysis products used in this study. We also appreciate all anonymous reviewers for  
851 their [insightful constructive](#) and [insightful valuable](#) comments.

852

## 853 **References**

- 854 Alfaro, S. C., Lafon, S., Rajot, J. L., Formenti, P., Gaudichet, A., and Maillé, M.: Iron oxides and  
855 light absorption by pure desert dust: An experimental study, *J. Geophys. Res.*, 109, D08208,  
856 doi:10.1029/2003JD004374, 2004.
- 857 Anderson, T. L., Covert, D. S., Marshall, S. F., Laucks, M. L., Charlson, R. J., Waggoner, A. P.,  
858 Ogren, J. A., Caldow, R., Holm, R. L., Quant, F. R., Sem, G. J., Wiedensohler, A., Ahlquist, N.  
859 A., and Bates, T. S.: Performance characteristics of a high-sensitivity, three-wavelength total  
860 scatter-backscatter nephelometer, *J. Atmos. Oceanic Technol.*, 13: 967–986, 1996.
- 861 Anderson, T. L. and Ogren, J. A.: Determining aerosol radiative properties using the TSI 3563

862 Integrating Nephelometer, *Aerosol Sci. Technol.*, 29, 57–69, doi:10.1080/02786829808965551,  
863 1998.

864 Anderson, T. L., Masonis, S. J., Covert, D. S., Ahlquist, N. C., Howell, S. G., Clarke, A. D., and  
865 McNaughton, C. S.: Variability of aerosol optical properties derived from in situ aircraft  
866 measurements during ACE–Asia, *J. Geophys. Res.*, 108(D23), 8647,  
867 doi:10.1029/2002JD003247, 2003.

868 Aoki, I., Kurosaki, Y., Osada, R., Sato, T., and Kimura, F.: Dust storms generated by mesoscale  
869 cold fronts in the Tarim Basin, Northwest China, *Geophys. Res., Lett.*, 32, L06807,  
870 doi:10.1029/2004GL021776, 2005.

871 Aoki, T., Motoyoshi, H., Kodama, Y., Yasunari, T. J., Sugiura, K., and Kobayashi, H.:  
872 Atmospheric aerosol deposition on snow surfaces and its effect on albedo, *SOLA*, 2, 13–16,  
873 doi:10.2151/sola.2006–004, 2006.

874 Arimoto, R., Zhang, X. Y., Huebert, B. J., Kang, C. H., Savoie, D. L., Prospero, J. M., Sage, S. K.,  
875 Schloesslin, C. A., Khaing, H. M., and Oh, S. N.: Chemical composition of atmospheric  
876 aerosols from Zhenbeitai, China, and Gosan, South Korea, during ACE–Asia, *J. Geophys. Res.*,  
877 109, D19S04, doi:10.1029/2003JD004323, 2004.

878 Arimoto, R., Kim, Y. J., Kim, Y. P., Quinn, P. K., Bates, T. S., Anderson, T. L., Gong, S., Uno, I.,  
879 Chin, M., Huebert, B. J., Clarke, A. D., Shinozuka, Y., Weber, R. J., Anderson, J. R., Guazzotti,  
880 S. A., Sullivan, R. C., Sodeman, D. A., Prather, K. A., and Sokolik, I. N.: Characterization of  
881 Asian dust during ACE–Asia, *Global Planet. Change*, 52, 23–56,  
882 doi:10.1016/j.gloplacha.2006.02.013, 2006.

883 Arya, S. P.: *Air Pollution Meteorology and Dispersion*, 310 pp., Oxford University Press, New  
884 York, 1999.

885 Bergin, M. H., Cass, G. R., Xu, J., Fang, C., Zeng, L. M., Yu, T., Salmon, L. G., Kiang, C. S., Tang,  
886 X. Y., Zhang, Y. H., and Chameides, W. L.: Aerosol radiative, physical, and chemical properties  
887 in Beijing during June 1999, *J. Geophys. Res.*, 106(D16), 17969–17980, doi:  
888 10.1029/2001JD900073, 2001.

889 Bi, J., Huang, J., Fu, Q., Wang, X., Shi, J., Zhang, W., Huang, Z., and Zhang B.: Toward  
890 characterization of the aerosol optical properties over Loess Plateau of Northwestern China, *J.*  
891 *Quant. Spectrosc. Radiat. Transfer.*, 112, 346–360, doi:10.1016/j.jqsrt.2010.09.006, 2011.

892 Bi, J., Huang, J., Fu, Q., Ge, J., Shi, J., Zhou, T., and Zhang, W.: Field measurement of clear-sky  
893 solar irradiance in Badain Jaran Desert of Northwestern China, *J. Quant. Spectrosc. Radiat.*  
894 *Transf.*, 122, 194–207, doi:10.1016/j.jqsrt.2012.07.025, 2013.

895 Bi, J., Shi, J., Xie, Y., Liu, Y., Takamura, T., and Khatri, P.: Dust aerosol characteristics and  
896 shortwave radiative impact at a Gobi Desert of Northwest China during the spring of 2012, *J.*  
897 *Meteor. Soc. Jpn, Ser. II*, 92A, 33–56, DOI:10.2151/jmsj.2014-A03, 2014.

898 Bi, J., Huang, J., Holben, B., and Zhang, G.: Comparison of key absorption and optical properties  
899 between pure and transported anthropogenic dust over East and Central Asia, *Atmos. Chem.*  
900 *Phys.*, 16, 15501–15516, doi:10.5194/acp-16-15501-2016, 2016.

901 Campbell, J. R., Hlavka, D. L., Welton, E. J., Flynn, C. J., Turner, D. D., Spinhirne, J. D., Scott, V.  
902 S., and Hwang, I. H.: Full-Time, eye-safe cloud and aerosol lidar observation at Atmospheric  
903 Radiation Measurement program sites: Instruments and data processing, *J. Atmos. Oceanic*  
904 *Technol.*, 19, 431–442, doi:10.1175/1520-0426(2002)019<0431:FTESCA>2.0.CO;2, 2002.

905 Cao, J. J., Lee, S. C., Zhang, X. Y., Chow, J. C., An, Z. S., Ho, K. F., Watson, J. G., Fung, K.,  
906 Wang, Y. Q., and Shen, Z. X.: Characterization of airborne carbonate over a site on Asian dust  
907 source regions during 2002 spring and its climatic and environmental significance, *J. Geophys.*  
908 *Res.*, 110, D03203, doi:10.1029/2004JD005244, 2005.

909 Che, H., Zhang, X. Y., Chen, H. B., Damiri, B., Goloub, P., Li, Z., Zhang, X., Wei, Y., Zhou, H.,  
910 Dong, F., Li, D., and Zhou, T.: Instrument calibration and aerosol optical depth validation of the  
911 China Aerosol Remote Sensing Network, *J. Geophys. Res.*, 114, D03206,  
912 doi:10.1029/2008JD011030, 2009.

913 Che, H., Zhang, X.-Y., Xia, X., Goloub, P., Holben, B., Zhao, H., Wang, Y., Zhang, X.-C., Wang,  
914 H., Blarel, L., Damiri, B., Zhang, R., Deng, X., Ma, Y., Wang, T., Geng, F., Qi, B., Zhu, J., Yu,  
915 J., Chen, Q., and Shi, G.: Ground-based aerosol climatology of China: aerosol optical depths  
916 from the China Aerosol Remote Sensing Network (CARSNET) 2002–2013, *Atmos. Chem.*  
917 *Phys.*, 15, 7619–7652, doi:10.5194/acp-15-7619-2015, 2015.

918 Cheng, T., Lu, D., Wang, G., and Xu, Y.: Chemical characteristics of Asian dust aerosol from  
919 Hunshan Dake Sandland in Northern China, *Atmos. Environ.*, 39, 2903–2911,  
920 doi:10.1016/j.atmosenv.2004.12.045, 2005.

921 Covert, D. S., Charlson, R. J., and Ahlquist, N. C.: A study of the relationship of chemical

922 composition and humidity to light scattering by aerosols, *J. Appl. Meteo.*, 11: 968–976, 1972.

923 Creamean, J. M., Suski, K. J., Rosenfeld, D., Cazorla, A., DeMott, P. J., Sullivan, R. C., White, A.  
924 B., Ralph, F. M., Minnis, P., Comstock, J. M., Tomlinson, J. M., and Prather, K. A.: Dust and  
925 biological aerosols from the Sahara and Asia influence precipitation in the western U.S.,  
926 *Science*, 339, 1572–1578, doi:10.1126/science.1227279, 2013.

927 Delene, D. and Ogren, J. A.: Variability of aerosol optical properties at four North American  
928 surface monitoring sites, *J. Atmos. Sci.*, 59(6), 1135–1150,  
929 doi:10.1175/1520-0469(2002)059<1135:VOAOPA>2.0.CO;2, 2002.

930 Dubovik, O., Holben, B. N., Eck, T. F., Smirnov, A., Kaufman, Y. J., King, M. D., Tanré, D., and  
931 Slutsker, I.: Variability of absorption and optical properties of key aerosol types observed in  
932 worldwide locations, *J. Atmos. Sci.*, 59, 590–608, 2002.

933 Eck, T. F., Holben, B. N., Dubovik, O., Smirnov, A., Goloub, P., Chen, H. B., Chatenet, B., Gomes,  
934 L., Zhang, X.-Y., Tsay, S.-C., Ji, Q., Giles, D., and Slutsker, I.: Columnar aerosol optical  
935 properties at AERONET sites in central eastern Asia and aerosol transport to the tropical  
936 mid-Pacific, *J. Geophys. Res.*, 110, D06202, doi:10.1029/2004JD005274, 2005.

937 Ge, J., Su, J., Ackerman, T. P., Fu, Q., Huang, J., and Shi, J.: Dust aerosol optical properties  
938 retrieval and radiative forcing over northwest China during the 2008 China–U.S. joint field  
939 experiment, *J. Geophys. Res.*, 115, D00K12, doi:10.1029/2009JD013263, 2010.

940 Ge, J., Liu, H., Huang, J., and Fu, Q.: Taklimakan Desert nocturnal low-level jet: climatology and  
941 dust activity, *Atmos. Chem. Phys.*, 16, 7773–7783, doi:10.5194/acp-16-7773-2016, 2016.

942 Ginoux, P., Prospero, J. M., Gill, T. E., Hsu, N. C., and Zhao, M.: Global-scale attribution of  
943 anthropogenic and natural sources and their emission rates based on MODIS Deep Blue aerosol  
944 products, *Rev. Geophys.*, 50, RG3005, doi:10.1029/2012RG000388, 2012.

945 Guan, X., Huang, J., Zhang, Y., Xie, Y., and Liu, J.: The relationship between anthropogenic dust  
946 and population over global semi-arid regions, *Atmos. Chem. Phys.*, 16, 5159–5169,  
947 doi:10.5194/acp-16-5159-2016, 2016.

948 Hansen, J., Sato, M., and Ruedy, R.: Radiative forcing and climate response, *J. Geophys. Res.*, 102,  
949 6831–6864, 1997.

950 Holben, B. N., Eck, T. F., Slutsker, I., Tanre, D., Buis, J. P., Setzer, A., Vermote, E., Reagan, J. A.,  
951 Kaufman, Y. J., Nakajima, T., Lavenu, F., Jankowiak, F., and Smirnov, A., AERONET—A



952 federated instrument network and data archive for aerosol characterization, *Remote Sens.*  
953 *Environ.*, 66, 1–16, 1998.

954 Huang, J., Minnis, P., Lin, B., Yi, Y., Khaiyer, M. M., Arduini, R. F., Fan, A., and Mace, G. G.:  
955 Advanced retrievals of multilayered cloud properties using multispectral measurements, *J.*  
956 *Geophys. Res.*, 110, D15S18, doi:10.1029/2004JD005101, 2005.

957 Huang, J., Lin, B., Minnis, P., Wang, T., Wang, X., Hu, Y., Yi, Y., and Ayers, J. K.: Satellite-based  
958 assessment of possible dust aerosols semi-direct effect on cloud water path over East Asia,  
959 *Geophys. Res. Lett.*, 33, L19802, doi:10.1029/2006GL026561, 2006.

960 Huang, J., Minnis, P., Chen, B., Huang, Z., Liu, Z., Zhang, Q., Yi, Y., and Ayers, J. K.: Long-range  
961 transport and vertical structure of Asian dust from CALIPSO and surface measurements during  
962 PACDEX, *J. Geophys. Res.*, 113, D23212, doi:10.1029/2008JD010620, 2008a.

963 Huang, J., Zhang, W., Zuo, J., Bi, J., Shi, J., Wang, X., Chang, Z., Huang, Z., Yang, S., Zhang, B.,  
964 Wang, G., Feng, G., Yuan, J., Zhang, L., Zuo, H., Wang, S., Fu, C., and Chou, J.: An overview of  
965 the semi-arid climate and environment research observatory over the Loess Plateau, *Adv.*  
966 *Atmos. Sci.*, 25, 906–921, doi:10.1007/s00376-008-0906-7, 2008b.

967 Huang, J., Fu, Q., Su, J., Tang, Q., Minnis, P., Hu, Y., Yi, Y., and Zhao, Q.: Taklimakan dust  
968 aerosol radiative heating derived from CALIPSO observations using the Fu–Liou radiation  
969 model with CERES constraints, *Atmos. Chem. Phys.*, 9, 4011–4021,  
970 doi:10.5194/acp-9-4011-2009, 2009.

971 Huang, J., Minnis, P., Yan, H., Yi, Y., Chen, B., Zhang, L., and Ayers, J. K.: Dust aerosol effect on  
972 semi-arid climate over Northwest China detected from A-Train satellite measurements, *Atmos.*  
973 *Chem. Phys.*, 10, 6863–6872, doi:10.5194/acp-10-6863-2010, 2010.

974 Huang, J., Fu, Q., Zhang, W., Wang, X., Zhang, R., Ye, H., and Warren, S. G.: Dust and black  
975 carbon in seasonal snow across northern China, *Bull. Amer. Meteor. Soc.*, 92, 175–181,  
976 doi:10.1175/2010BAMS3064.1, 2011.

977 Huang, J., Wang, T., Wang, W., Li, Z., and Yan, H.: Climate effects of dust aerosols over East  
978 Asian arid and semiarid regions, *J. Geophys. Res.*, 119, 11398–11416,  
979 doi:10.1002/2014JD021796, 2014.

980 Huang, J. P., Liu, J. J., Chen, B., and Nasiri, S. L.: Detection of anthropogenic dust using  
981 CALIPSO lidar measurements, *Atmos. Chem. Phys.*, 15, 11653–11665,

982 doi:10.5194/acp-15-11653-2015, 2015.

983 Huang, J., Yu, H., Guan, X., Wang, G., and Guo, R.: Accelerated dryland expansion under climate  
984 change, *Nature Clim. Change*, 6(2), 166–171, doi:10.1038/nclimate2837, 2016.

985 Huang, K., Zhuang, G., Li, J., Wang, Q., Sun, Y., Lin, Y., and Fu, J. S.: Mixing of Asian dust with  
986 pollution aerosol and the transformation of aerosol components during the dust storm over  
987 China in spring 2007, *J. Geophys. Res.*, 115, D00K13, doi:10.1029/2009JD013145, 2010.

988 Huang, Z., Huang, J., Bi, J., Wang, G., Wang, W., Fu, Q., Li, Z., Tsay, S.-C., and Shi, J.: Dust  
989 aerosol vertical structure measurements using three MPL lidars during 2008 China–U.S. joint  
990 dust field experiment, *J. Geophys. Res.*, 115, D00K15, doi:10.1029/2009JD013273, 2010.

991 Huebert, B. J., Bates, T., Russell, P. B., Shi, G., Kim, Y. J., Kawamura, K., Carmichael, G., and  
992 Nakajima, T.: An overview of ACE–Asia: Strategies for quantifying the relationships between  
993 Asian aerosols and their climatic impacts, *J. Geophys. Res.*, 108(D23), 8633,  
994 doi:10.1029/2003JD003550, 2003.

995 Intergovernmental Panel on Climate Change (IPCC): *Climate Change 2013: The Physical Science*  
996 *Basis, Contribution of Working Group I to the Fifth Assessment Report of the Intergovernmental*  
997 *Panel on Climate Change*, edited by Stocker, T. F., Qin, G., Plattner, M., Tignor, S. K.  
998 Allen, J. Boschung, A. Nauels, Y. Xia, V. Bex and P. M. Midgley. Cambridge University Press,  
999 Cambridge, United Kingdom and New York, NY, USA, 1535 pp, 2013.

1000 Jickells, T., An, Z., Andersen, K., Baker, A., Bergametti, G., Brooks, N., Cao, J., Boyd, P., Duce,  
1001 R., Hunter, K., Kawahata, H., Kubilay, N., laRoche, J., Liss, P., Mahowald, N., Prospero, J.,  
1002 Ridgwell, A., Tegen, I., and Torres, R.: Global iron connections between desert dust, ocean  
1003 biogeochemistry, and climate, *Science*, 308, 67–71, doi:10.1126/science.1105959, 2005.

1004 Kai, K., Nagata, Y., Tsunematsu, N., Matsumura, T., Kim, H.-S., Matsumoto, T., Hu, S., Zhou, H.,  
1005 Abo, M., and Nagai, T.: The structure of the dust layer over the Taklimakan Desert during the  
1006 dust storm in April 2002 as observed using a depolarization lidar, *J. Meteor. Soc. Jpn*, 86(1),  
1007 1–16, doi:10.2151/jmsj.86.1, 2008.

1008 Khatri, P. and Takamura, T.: An algorithm to screen cloud-affected data for sky radiometer data  
1009 analysis, *J. Meteor. Soc. Jpn*, 87, 189–204, doi:10.2151/jmsj.87.189, 2009.

1010 Kobayashi, A., Hayashida, S., Okada, K., and Iwasaka, Y.: Measurements of the polarization  
1011 properties of Kosa (Asian Dust storm) particles by a Laser Radar in spring 1983, *J. Meteor. Soc.*,

1012 Jpn., 63, 144–149, 1985.

1013 Lafon, S., Rajot, J.–L., Alfaro, S. C., and Gaudichet, A.: Quantification of iron oxides in desert  
1014 aerosol, *Atmos. Environ.*, 38, 1211–1218, 2004.

1015 Lafon, S., Sokolik, I. N., Rajot, J. L., Caquineau, S., and Gaudichet, A.: Characterization of iron  
1016 oxides in mineral dust aerosols: Implications for light absorption, *J. Geophys. Res.*, 111,  
1017 D21207, doi:10.1029/2005JD007016, 2006.

1018 Li, C., Marufu, L. T., Dickerson, R. R., Li, Z., Wen, T., Wang, Y., Wang, P., Chen, H., and Stehr, J.  
1019 W.: In situ measurements of trace gases and aerosol optical properties at a rural site in northern  
1020 China during East Asian Study of Tropospheric Aerosols: An International Regional Experiment  
1021 2005, *J. Geophys. Res.*, 112, D22S04, doi:10.1029/2006JD007592, 2007.

1022 Li, C., Tsay, S.–C., Fu, J. S., Dickerson, R. R., Ji, Q., Bell, S. W., Gao, Y., Zhang, W., Huang, J., Li,  
1023 Z., and Chen, H.: Anthropogenic air pollution observed near dust source regions in  
1024 northwestern China during springtime 2008, *J. Geophys. Res.*, 115, D00K22,  
1025 doi:10.1029/2009JD013659, 2010.

1026 Li, W. J. and Shao, L. Y.: Observation of nitrate coatings on atmospheric mineral dust particles,  
1027 *Atmos. Chem. Phys.*, 9, 1863–1871, doi:10.5194/acp-9-1863-2009, 2009.

1028 Li, Z., Li, C., Chen, H., Tsay, S.–C., Holben, B., Huang, J., Li, B., Maring, H., Qian, Y., Shi, G.,  
1029 Xia, X., Yin, Y., Zheng, Y., and Zhuang, G.: East Asian Studies of Tropospheric Aerosols and  
1030 their Impact on Regional Climate (EAST–AIRC): An overview, *J. Geophys. Res.*, 116, D00K34,  
1031 doi:10.1029/2010JD015257, 2011.

1032 Li, Z., Lau, W. K.–M., Ramanathan, V., Wu, G., Ding, Y., Manoj, M. G., Liu, J., Qian, Y., Li, J.,  
1033 Zhou, T., Fan, J., Rosenfeld, D., Ming, Y., Wang, Y., Huang, J., Wang, B., Xu, X., Lee, S.–S.,  
1034 Gribb, M., Zhang, F., Yang, X., Zhao, C., Takemura, T., Wang, K., Xia, X., Yin, Y., Zhang, H.,  
1035 Guo, J., Zhai, P. M., Sugimoto, N., Babu, S. S., and Brasseur, G. P.: Aerosol and monsoon  
1036 climate interactions over Asia, *Rev. Geophys.*, 54, doi:10.1002/2015RG000500, 2016.

1037 Ma, J., He, J., Qi, S., Zhu, G., Zhao, W., Edmunds, W. M., and Zhao, Y.: Groundwater recharge  
1038 and evolution in the Dunhuang Basin, northwestern China, *Appl. Geochem.*, 28, 19–31,  
1039 doi:10.1016/j.apgeochem.2012.10.007, 2013.

1040 Maher, B. A., Prospero, J. M., Mackie, D., Gaiero, D., Hesse, P. P., and Balkanski, Y.: Global  
1041 connections between aeolian dust, climate and ocean biogeochemistry at the present day and at

1042 the last glacial maximum, *Earth–Sci. Rev.*, 99 (1–2), pp. 61–97,  
1043 doi:10.1016/j.earscirev.2009.12.001, 2010.

1044 Mikami, M., Shi, G. Y., Uno, I., Yabuki, S., Iwasaka, Y., Yasui, M., Aoki, T., Tanaka, T. Y.,  
1045 Kurosaki, Y., Masuda, K., Uchiyama, A., Matsuki, A., Sakai, T., Takemi, T., Nakawo, M., Seino,  
1046 N., Ishizuka, M., Satake, S., Fujita, K., Hara, Y., Kai, K., Kanayama, S., Hayashi, M., Du, M.,  
1047 Kanai, Y., Yamada, Y., Zhang, X. Y., Shen, Z., Zhou, H., Abe, Q., Nagai, T., Tsutsumi, Y., Chiba,  
1048 M., and Suzuki, J.: Aeolian dust experiment on climate impact: An overview of Japan–China  
1049 joint project ADEC, *Global Planet. Change*, 52, 142–172, doi:10.1016/j.gloplacha.2006.03.001,  
1050 2006.

1051 Murayama, T., Okamoto, H., Kaneyasu, N., Kamataki, H., and Miura, K.: Application of lidar  
1052 depolarization measurement in the atmospheric boundary layer: Effects of dust and sea-salt  
1053 particles, *J. Geophys. Res.*, 104, 31781–31792, 1999.

1054 Nakajima, T., Tonna, G., Rao, R., Boi, P., Kaufman, Y., and Holben, B.: Use of sky brightness  
1055 measurements from ground for remote sensing of particulate polydispersions, *Appl. Opt.*,  
1056 35(15), 2672–2686, doi:10.1364/AO.35.002672, 1996.

1057 Nakajima, T., Sekiguchi, M., Takemura, T., Uno, I., Higurashi, A., Kim, D., Sohn, B. J., Oh, S.  
1058 –N., Nakajima, T. Y., Ohta, S., Okada, I., Takamura, T., and Kawamoto, K.: Significance of  
1059 direct and indirect radiative forcings of aerosols in the East China Sea region, *J. Geophys. Res.*,  
1060 108(D23), 8658, doi:10.1029/2002JD003261, 2003.

1061 Nie, W., Ding, A., Wang, T., Kerminen, V.-M., George, C., Xue, L., Wang, W., Zhang, Q., Petäjä,  
1062 T., Qi, X., Gao, X., Wang, X., Yang, X., Fu, C., and Kulmala, M.: Polluted dust promotes new  
1063 particle formation and growth, *Sci. Rep.*, 4: 6634, DOI:10.1038/srep06634, 2014.

1064 Petzold, A., Kramer, H., and Schönlinner, M.: Continuous measurement of atmospheric black  
1065 carbon using a multi - angle absorption photometer, *Environ. Sci. Poll. Res.*, 4: 78–82, 2002.

1066 Petzold, A., Schloesser, H., Sheridan, P. J., Arnott, W. P., Ogren, J. A., and Virkkula A.: Evaluation  
1067 of multiangle absorption photometry for measuring aerosol light absorption, *Aerosol Sci. Tech.*,  
1068 39:1, 40–51, doi:10.1080/027868290901945, 2005.

1069 Qian, Y., Yasunari, T. J., Doherty, S. J., Flanner, M. G., Lau, W. K.-M., Ming, J., Wang, H., Wang,  
1070 M., Warren, S. G., and Zhang, R.: Light-absorbing particles in snow and ice: Measurement and  
1071 modeling of climatic and hydrological impact, *Adv. Atmos. Sci.*, 32, 64–91,

1072 doi:10.1007/s00376-014-0010-0, 2014.

1073 Ramanathan, V., Crutzen, P. J., Kiehl, J. T., and Rosenfeld, D.: Aerosols, climate, and the  
1074 hydrological cycle, *Science*, 294, 2119–2124, doi:10.1126/science.1064034, 2001.

1075 Rienecker, M. M., Suarez, M. J., Gelaro, R., Todling, R., Bacmeister, J., Liu, E., Bosilovich, M. G.,  
1076 Schubert, S. D., Takacs, L., Kim, G-K., Bloom, S., Chen, J., Collins, D., Conaty, A., Silva, A.  
1077 da, Gu, W., Joiner, J., Koster, R. D., Lucchesi, R., Molod, A., Owens, T., Pawson, S., Pegion, P.,  
1078 Redder, C. R., Reichle, R., Robertson, F. R., Ruddick, A. G., Sienkiewicz, M., and Woollen, J.:  
1079 MERRA: NASA's Modern-Era Retrospective Analysis for Research and Applications, *J.*  
1080 *Climate*, 24, 3624–3648. doi: 10.1175/JCLI-D-11-00015.1, 2011.

1081 Rosenfeld, D., Rudich, Y., and Lahav, R.: Desert dust suppressing precipitation: A possible  
1082 desertification feedback loop, *Proc. Natl. Acad. Sci. U.S.A.*, 98, 5975–5980, 2001.

1083 Shao, Y., Wyrwoll, K.-H., Chappel, A., Huang, J., Lin, Z., McTainsh, G., Mikami, M., Tanaka, T.,  
1084 Wang, X., and Yoon, S.: Dust cycle: An emerging core theme in Earth system science, *Aeolian*  
1085 *Res.*, 2, 181–204, 2011.

1086 Shimizu, A., Sugimoto, N., Matsui, I., Arao, K., Uno, I., Murayama, T., Kagawa, N., Aoki, K.,  
1087 Uchiyama, A., and Yamazaki, A.: Continuous observations of Asian dust and other aerosol by  
1088 polarization lidars in China and Japan during ACE-Asia, *J. Geophys. Res.*, 109, D19S17,  
1089 doi:10.1029/2002JD003253, 2004.

1090 Sokolik, I. N. and Toon, O. B.: Incorporation of mineralogical composition into models of the  
1091 radiative properties of mineral aerosol from UV to IR wavelengths, *J. Geophys. Res.*, 104, D8,  
1092 9423–9444, 1999.

1093 Sun, J., Zhang, M., and Liu, T.: Spatial and temporal characteristics of dust storms in China and its  
1094 surrounding regions, 1960–1990: Relations to source area and climate, *J. Geophys. Res.*,  
1095 106(D10), 10325–10333, doi:10.1029/2000JD900665, 2001.

1096 Takamura, T., Nakajima, T., and SKYNET community group: Overview of SKYNET and its  
1097 Activities, *Opt. Puray Apl.*, 37, 3303–3308, 2004.

1098 Tegen, I. and Fung, I.: Contribution to the atmospheric mineral aerosol load from land surface  
1099 modification, *J. Geophys. Res.*, 100, 18707–18726, doi:10.1029/95JD02051, 1995.

1100 Torres, O., Tanskanen, A., Veihelmann, B., Ahn, C., Braak, R., Bhartia, P. K., Veefkind, P., and  
1101 Levelt, P.: Aerosols and surface UV products from Ozone Monitoring Instrument observations:

1102 An overview, *J. Geophys. Res.*, 112, D24S47, doi:10.1029/2007JD008809, 2007.

1103 Uchiyama, A., Yamazaki, A., Togawa, H., Asano, J., and Shi, G.-Y.: Single scattering albedo of  
 1104 Aeolian dust as inferred from sky-radiometer and in situ ground-based measurement, *SOLA*,  
 1105 Vol. 1, pp. 209–212, doi:10.2151/sola.2005-054, 2005.

1106 Uno, I., Eguchi, K., Yumimoto, K., Takemura, T., Shimizu, A., Uematsu, M., Liu, Z., Wang, Z.,  
 1107 Hara, Y., and Sugimoto, N.: Asian dust transported one full circuit around the globe, *Nature*  
 1108 *Geosci.*, 2, 557–560, doi:10.1038/NGEO583, 2009.

1109 Uno, I., Eguchi, K., Yumimoto, K., Liu, Z., Hara, Y., Sugimoto, N., Shimizu, A., and Takemura, T.:  
 1110 Large Asian dust layers continuously reached North America in April 2010, *Atmos. Chem.*  
 1111 *Phys.*, 11, 7333–7341, 2011.

1112 Wang, G., Huang, J., Guo, W., Zuo, J., Wang, J., Bi, J., Huang, Z., and Shi, J.: Observation  
 1113 analysis of land-atmosphere interactions over the Loess Plateau of northwest China, *J. Geophys.*  
 1114 *Res.*, 115, D00K17, doi:10.1029/2009JD013372, 2010.

1115 Wang, K., and Dickinson, R. E.: Global atmospheric downward longwave radiation at the surface  
 1116 from ground-based observations, satellite retrievals, and reanalyses, *Rev. Geophys.*, 51,  
 1117 150–185, doi:10.1002/rog.20009, 2013.

1118 Wang, W., Huang, J., Minnis, P., Hu, Y., Li, J., Huang, Z., Ayers, J. K., and Wang, T.: Dusty cloud  
 1119 properties and radiative forcing over dust source and downwind regions derived from A-Train  
 1120 data during the Pacific Dust Experiment, *J. Geophys. Res.*, 115, D00H35,  
 1121 doi:10.1029/2010JD014109, 2010.

1122 Wang, X., Huang, J., Ji, M., and Higuchi, K.: Variability of East Asia dust events and their  
 1123 long-term trend, *Atmos. Environ.*, 42, 13, 3156–3165, doi:10.1016/j.atmosenv.2007.07.046,  
 1124 2008.

1125 Wang, X., Doherty, S. J., and Huang, J.: Black carbon and other light-absorbing impurities in  
 1126 snow across Northern China, *J. Geophys. Res.*, 118, 1471–1492, doi:10.1029/2012JD018291,  
 1127 2013.

1128 Wang, X., Pu, W., Shi, J., Bi, J., Zhou, T., Zhang, X., and Ren, Y.: A comparison of the physical  
 1129 and optical properties of anthropogenic air pollutants and mineral dust over Northwest China, *J.*  
 1130 *Meteorol. Res.*, 29, 180–200, doi:10.1007/s13351-015-4092-0, 2015.

1131 Welton, E. J., Voss, K. J., Gordon, H. R., Maring, H., Smirnov, A., Holben, B., Schmid, B.,

1132 Livingston, J. M., Russell, P. B., Durkee, P. A., Formenti, P., and Andreae, M. O.: Ground-based  
1133 lidar measurements of aerosols during ACE-2: Instrument description, results, and comparisons  
1134 with other ground-based and airborne measurements, *Tellus B*, 52, 636–651,  
1135 doi:10.1034/j.1600-0889.2000.00025.x, 2000.

1136 Wu, G. X., Li, Z. Q., Fu, C. B., Zhang, X. Y., Zhang, R. Y., Zhang, R. H., Zhou, T. J., Li, J. P., Li, J.  
1137 D., Zhou, D. G., Wu, L., Zhou, L. T., He, B., and Huang, R. H.: Advances in studying  
1138 interactions between aerosols and monsoon in China, *Sci. China Earth Sci.*, 59: 1,  
1139 doi:10.1007/s11430-015-5198-z, 2016.

1140 Xia, X., Zong, X., Cong, Z., Chen, H., Kang, S., and Wang, P.: Baseline continental aerosol over  
1141 the central Tibetan plateau and a case study of aerosol transport from South Asia, *Atmos.*  
1142 *Environ.*, 45, 7370–7378, doi:10.1016/j.atmosenv.2011.07.067, 2011.

1143 Xu, J., Bergin, M. H., Yu, X., Liu, G., Zhao, J., Marrico, C. M., and Baumann, K.: Measurement of  
1144 aerosol chemical, physical, and radiative properties in the Yangtze delta region of China, *Atmos.*  
1145 *Environ.*, 36, 161–173, doi:10.1016/S1352-2310(01)00455-1, 2002.

1146 Xu, J., Bergin, M. H., Greenwald, R., Schauer, J. J., Shafer, M. M., Jaffrezo, J. L., and Aymoz, G.:  
1147 Aerosol chemical, physical, and radiative characteristics near a desert source region of  
1148 northwest China during ACE-Asia, *J. Geophys. Res.*, 109, D19S03,  
1149 doi:10.1029/2003JD004239, 2004.

1150 Yan, H.: Aerosol scattering properties in northern China, *Atmos. Environ.*, 41, 6916–6922,  
1151 doi:10.1016/j.atmosenv.2007.04.052, 2007.

1152 Yan, P., Tang, J., Huang, J., Mao, J. T., Zhou, X. J., Liu, Q., Wang, Z. F., and Zhou, H. G.: The  
1153 measurement of aerosol optical properties at a rural site in Northern China, *Atmos. Chem. Phys.*,  
1154 8, 2229–2242, doi:10.5194/acp-8-2229-2008, 2008.

1155 Yin, Y. and Chen, L.: The effects of heating by transported dust layers on cloud and precipitation:  
1156 a numerical study, *Atmos. Chem. Phys.*, 7, 3497–3505, doi:10.5194/acp-7-3497-2007, 2007.

1157 Zhang, X., Arimoto, R., and An, Z.: Dust emission from Chinese desert sources linked to  
1158 variations in atmospheric circulation, *J. Geophys. Res.*, 102, D23, 28041–28047,  
1159 doi:10.1029/97JD02300, 1997.

1160 Zhao, T. L., Gong, S. L., Zhang, X. Y., Blanchet, J. -P., McKendry, I. G., and Zhou, Z. J.: A  
1161 simulated climatology of Asian Dust aerosol and its Trans-Pacific transport. Part I: Mean

1162 climate and validation, J. Climate, 19, 88–103, doi: 10.1175/JCLI3605.1, 2006.

1163

1164

1165

1166

1167

1168 **Figure captions**

1169

1170

1171 **Table 1.** The main aerosol observing and other ground-based instruments deployed at Dunhuang

1172 farmland during spring of 2012.

Measured variables	Model, Manufacturer	Accuracy
PM <sub>10</sub> concentration	Ambient particulate monitor (RP1400a), R&P Corp.	0.1 μgm <sup>-3</sup>
Aerosol scattering coefficient	Integrating nephelometer (TSI 3563), TSI Inc. 450, 550, and 700 nm	0.44, 0.17, and 0.26 Mm <sup>-1</sup>
Aerosol absorption coefficient	Multi-angle absorption photometer (MAAP 5012), Thermo	0.66 Mm <sup>-1</sup>
Aerosol size distribution	Aerodynamic particle sizer (APS 3321), TSI Inc., 0.5~20 μm	0.001 cm <sup>-3</sup>
Aerosol-attenuated backscatter profile	Micro-pulse lidar (MPL-4), Sigma Space Corp.	Spatial resolution: ~30 m
Meteorological elements	Weather transmitter (WXT-520), Vaisala, Ta, RH, P, u, WD	Ta: ±0.3°C, RH: 0.1%, P: 0.1 hPa, u: 0.1 ms <sup>-1</sup> , WD:1°
Global and diffuse radiation	Pyranometer (PSP <sup>a,b</sup> ), Eppley Lab., 0.285~2.8 μm	Global: 8.46, diffuse: 8.48 μVW <sup>-1</sup> m <sup>-2</sup>
Direct radiation	Pyrheliometer (NIP <sup>b</sup> ), Eppley Lab., 0.285~2.8 μm	8.38 μVW <sup>-1</sup> m <sup>-2</sup>
Downward long wave radiation	Pyrgeometer (PIR <sup>a,b</sup> ), Eppley Lab., 3.5~50 μm	2.98 μVW <sup>-1</sup> m <sup>-2</sup>
24-bit color JPEG image	Total Sky Imager (TSI880), YES Inc., 352×288 pixel	Sampling rate: 1 minute

1173 <sup>a</sup>The instrument is equipped with the Eppley ventilation system (VEN).

1174 <sup>b</sup>The instrument is mounted on a two-axis automatic sun tracker (Model 2AP, Kipp&Zonen).

1175

1176

1177 **Table 2.** Statistical summary of hourly average aerosol optical properties measured during

1178 intensive observation period<sup>a</sup>

Variable	Mean	Std <sup>b</sup>	Median	10 <sup>th</sup> percentile	25 <sup>th</sup> percentile	75 <sup>th</sup> percentile	90 <sup>th</sup> percentile
PM <sub>10</sub> (μgm <sup>-3</sup> )	113	169	54	17	29	111	300
σ <sub>sp</sub> (Mm <sup>-1</sup> )	53.3	74.8	28.3	11.2	16.0	55.8	123.5
σ <sub>ap</sub> (Mm <sup>-1</sup> )	3.20	2.40	2.50	1.27	1.69	3.90	5.94
SSA (670 nm)	0.913	0.055	0.923	0.850	0.892	0.949	0.967
SAE (450/700 nm)	0.45	0.45	0.42	-0.1	0.1	0.73	0.99



1179 <sup>a</sup>All aerosol data reported for volumes under 1013.25 hPa and 20 °C.

1180 <sup>b</sup>Std denotes the standard deviation.

1181

1182

1183

1184

1185

1186

1187

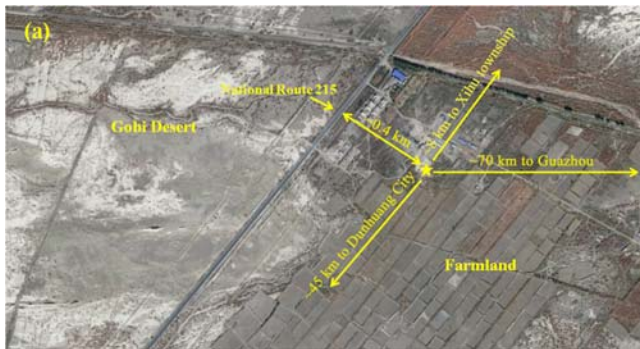
1188

1189

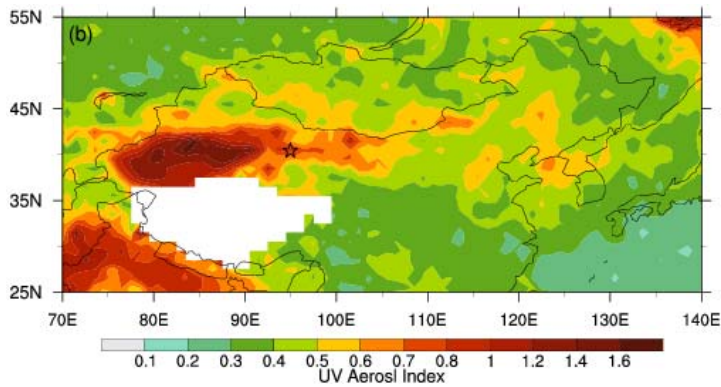
1190

1191

1192



1193



1194

1195 **Figure 1.** (a) The Dunhuang farmland site (40.492°N, 94.955°E, altitude: 1061 m) labeled with a

1196 pentagram and its surrounding region. (b) OMI (Ozone Monitoring Instrument, 2004) mean UV

1197 aerosol index from 1 April to 12 June 2012. The site is located in the downwind region of the

1198 Taklimakan Desert and frequently outbreaks dust storms.

1199

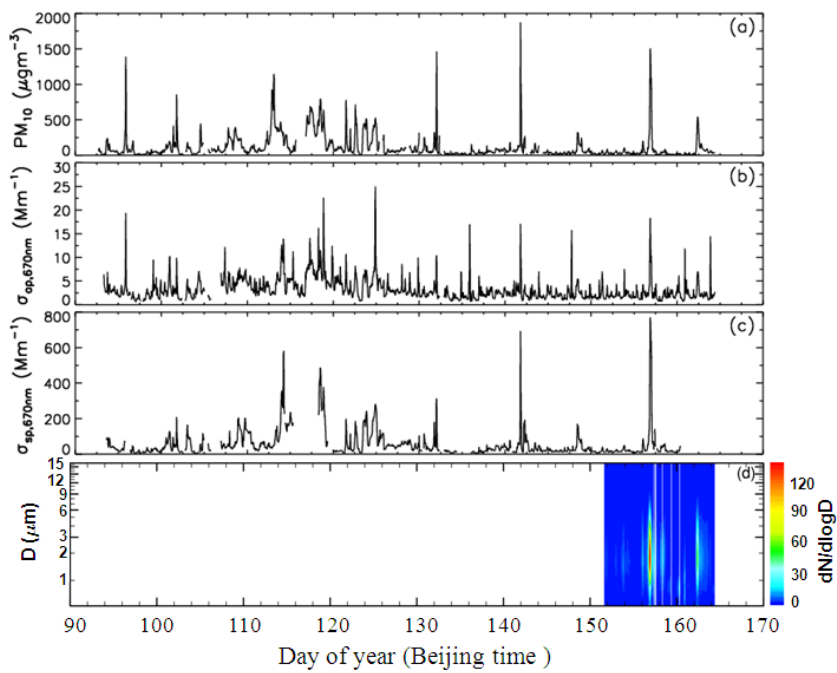
1200

1201

1202

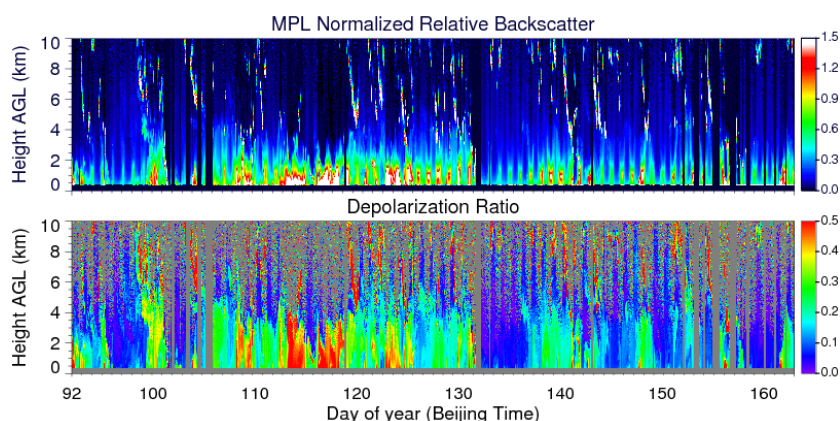
1203

1204  
1205  
1206  
1207  
1208  
1209  
1210  
1211  
1212



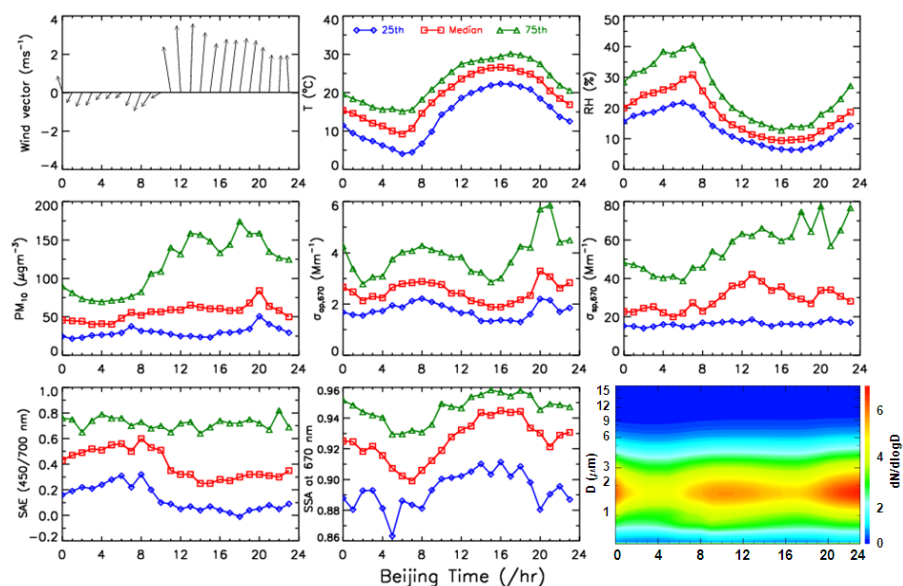
1213  
1214  
1215  
1216  
1217  
1218

**Figure 2.** Time series of hourly average (a) PM<sub>10</sub> mass concentration in  $\mu\text{g m}^{-3}$ , (b) aerosol absorption coefficient at 670 nm, (c) aerosol scattering coefficient at 670 nm, and (d) aerosol size distribution in  $\text{cm}^{-3}$  at Dunhuang farmland during the whole sampling period.



1219  
1220  
1221  
1222  
1223  
1224  
1225  
1226  
1227  
1228  
1229  
1230

**Figure 3.** Time evolutions of the MPL normalized relative backscatter intensity (top panel) and depolarization ratio (bottom panel) at Dunhuang farmland from 1 April to 12 June 2012.

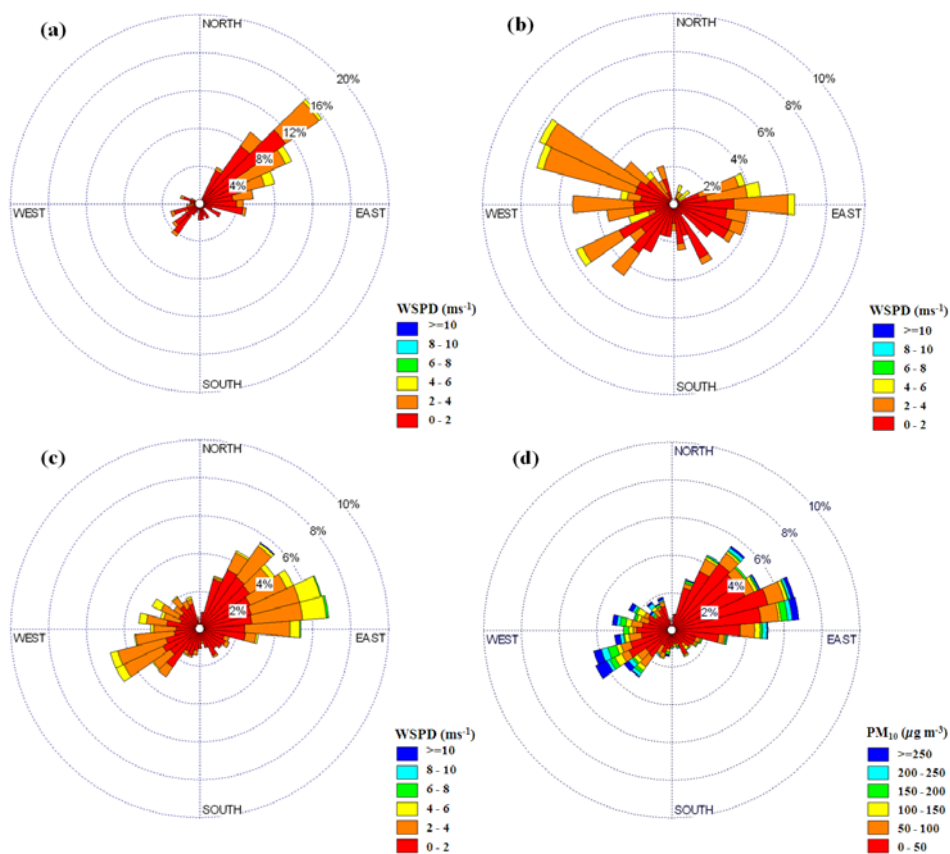


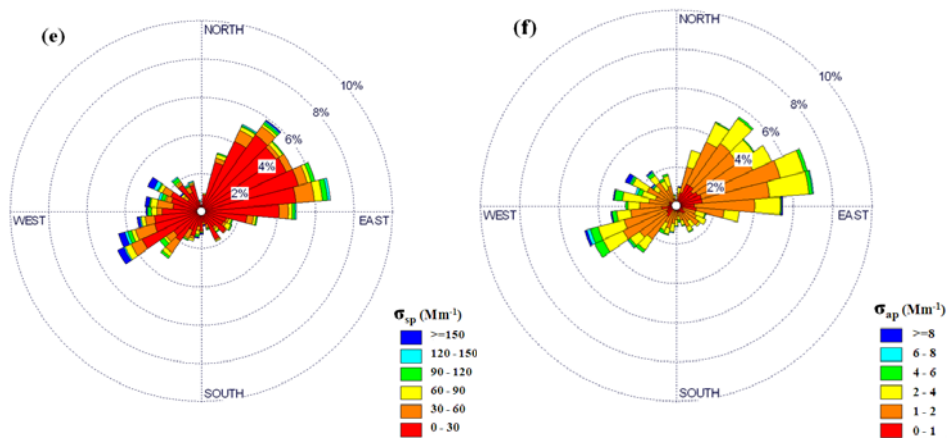
1231  
1232  
1233  
1234  
1235

**Figure 4.** The diurnal variations of (first row, left to right) wind vector ( $\text{ms}^{-1}$ ), air temperature ( $T$  in  $^{\circ}\text{C}$ ), relative humidity (RH in %), (second row, left to right)  $\text{PM}_{10}$  concentration ( $\mu\text{gm}^{-3}$ ), aerosol scattering coefficient at 670 nm ( $\sigma_{\text{sp},670}$  in  $\text{Mm}^{-1}$ ), aerosol absorption coefficient at 670 nm ( $\sigma_{\text{ap},670}$  in  $\text{Mm}^{-1}$ ), (third row, left to right) scattering Ångström exponent at 450–700 nm (SAE)

1236 450/700 nm), aerosol single-scattering albedo at 670 nm ( $SSA_{670}$ ), and aerosol size distribution  
 1237 ( $dN/d\log D$  in  $cm^{-3}$ ) in Dunhuang site from 1 April to 12 June 2012 (30 May to 12 June for aerosol  
 1238 size distribution). Median values (red square) are shown to give a more apparent diurnal feature  
 1239 than mean values, which could be affected by several strong dust episodes. The 25<sup>th</sup> (blue  
 1240 diamond) and 75<sup>th</sup> (green triangle) percentiles for each hour of the day are also displayed.

1241  
 1242  
 1243  
 1244  
 1245  
 1246  
 1247  
 1248  
 1249  
 1250  
 1251  
 1252  
 1253  
 1254





1257

1258

1259

1260

1261

1262

1263

1264

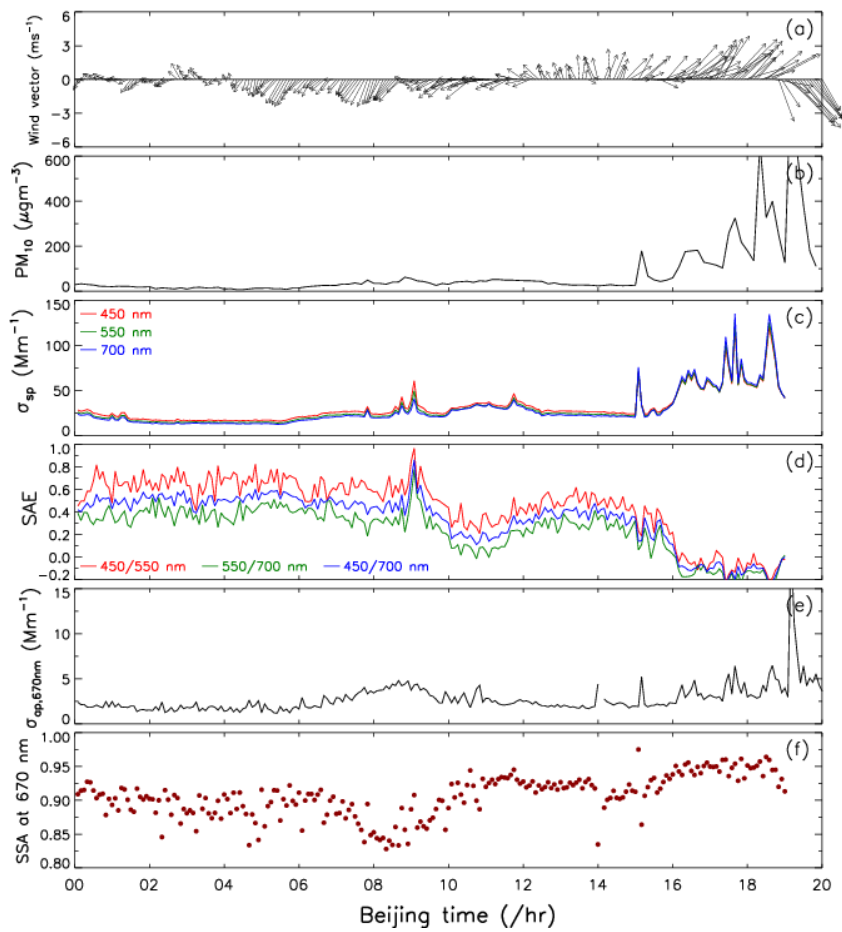
1265

1266

1267

1268

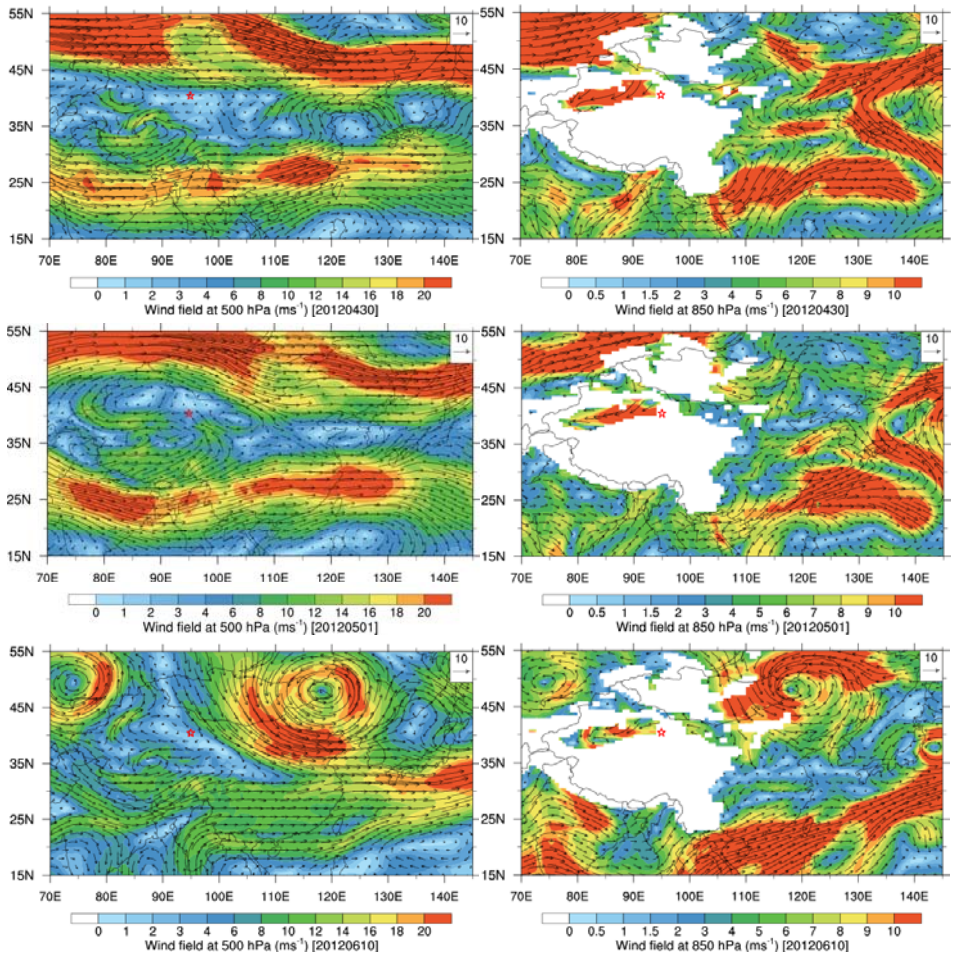
**Figure 5.** Wind rose plots for (a) morning hour (06:00–09:00 LT), (b) evening hour (19:00–22:00 LT), and (c) all hours; shade represents wind speed ( $\text{ms}^{-1}$ ). Wind roses for all hours, with shade representing levels of (d)  $\text{PM}_{10}$  concentration ( $\mu\text{g m}^{-3}$ ), (e) aerosol scattering coefficient at 670 nm ( $\sigma_{\text{sp}}$  in  $\text{Mm}^{-1}$ ), and (f) aerosol absorption coefficient at 670 nm ( $\sigma_{\text{ap}}$  in  $\text{Mm}^{-1}$ ).



1269  
 1270 **Figure 6.** Time series of (a) wind vector ( $\text{ms}^{-1}$ ), (b)  $\text{PM}_{10}$  concentration ( $\mu\text{g m}^{-3}$ ), (c) aerosol  
 1271 scattering coefficient ( $\sigma_{\text{sp}}$  in  $\text{Mm}^{-1}$ ) at 450 nm (red), 550 nm (green), and 700 nm (blue), (d)  
 1272 scattering Ångström exponent (SAE) at 450–550 nm (red), 550–700 nm (green), and 450–700 nm  
 1273 (blue), (e) aerosol absorption coefficient at 670 nm ( $\sigma_{\text{ap}}$  in  $\text{Mm}^{-1}$ ), and (f) single-albedo albedo at  
 1274 670 nm (SSA<sub>670</sub>) during a typical Tomb-sweeping Day on 4 April 2012, which implies a potential  
 1275 anthropogenic influence on aerosol optical properties. All data points are obtained from 5-minute  
 1276 average values.

1277  
 1278  
 1279  
 1280  
 1281  
 1282  
 1283  
 1284  
 1285  
 1286  
 1287





1288

1289

1290

1291

1292

1293

1294

1295

1296

1297

1298

1299

1300

1301

1302

1303

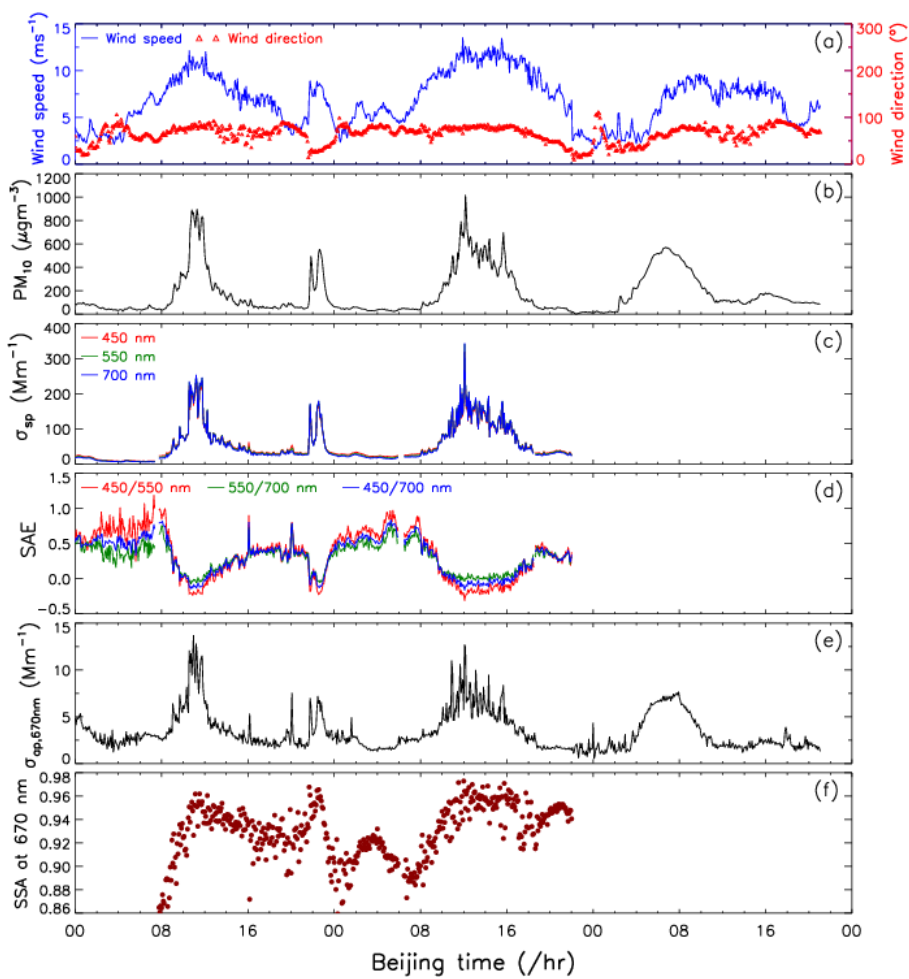
1304

1305

1306

1307

**Figure 7.** The wind fields (black arrows) at 500 hPa (left panel) and 850 hPa (right panel) levels during three heavy dust events on 30 April (top), 1 May (middle), and 10 June (bottom) 2012, based on MERRA reanalysis data. Note that the Dunhuang farmland is marked with a red pentagram and the white regions at 850 hPa are on behalf of the missing values.



1308

1309 **Figure 8.** The same as Figure 6, except for (a) wind speed (ms<sup>-1</sup>) and wind direction (°) during  
 1310 three heavy dust events on 30 April, 1 May, and 10 June 2012. There were no measurements of  
 1311 aerosol scattering coefficient (σ<sub>sp</sub> in Mm<sup>-1</sup>) on 10 June due to equipment failure.

1312

1313

1314

1315

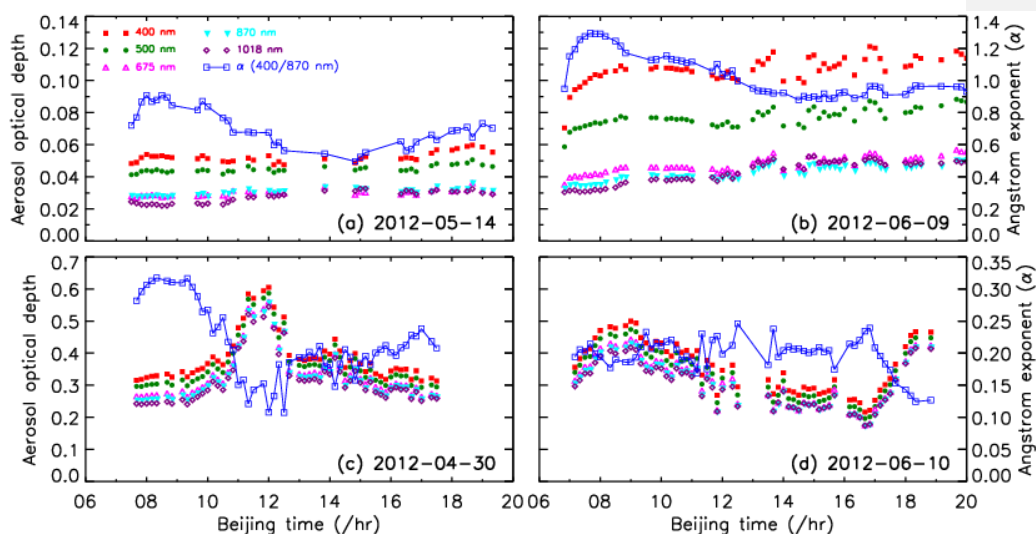
1316

1317

1318

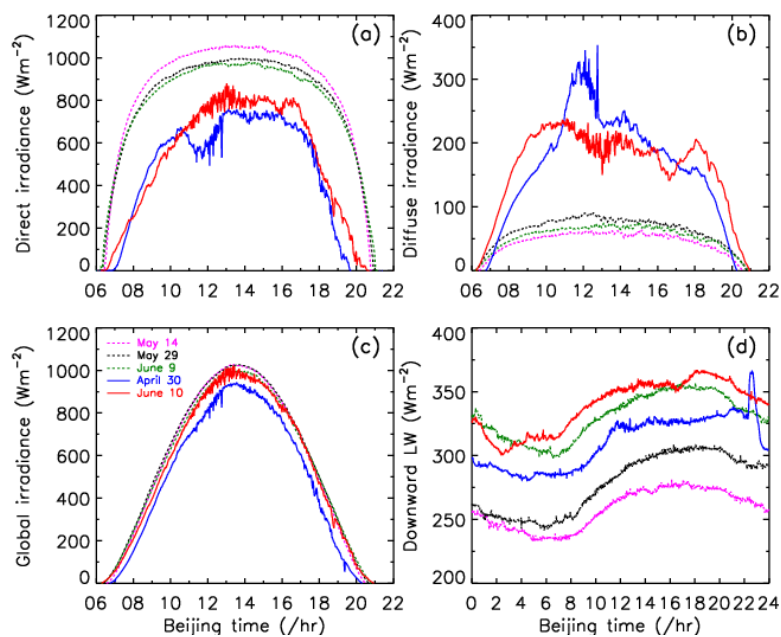
1319





1320  
1321  
1322  
1323  
1324  
1325  
1326

**Figure 9.** Time evolutions of aerosol optical depth (AOD) at five wavelengths (400, 500, 675, 870, and 1018 nm) versus Ångström exponent ( $\alpha$ ) at 400–870 nm on (a) 14 May, (b) 9 June, (c) 30 April, and (d) 10 June 2012. Note that Figures 9(a)–9(b) are adopted from *Bi et al.* (2014) with an addition of the Ångström exponent plot in the original publication.



1327  
1328  
1329  
1330  
1331

**Figure 10.** Diurnal variations of ground-based measured-measurements of 1-minute average (a) direct, (b) diffuse, and (c) global irradiances, and (d) downward long wave irradiance under completely clear-sky conditions (14 May, 29 May, and 9 June) and dust events (30 April and 10 June).